

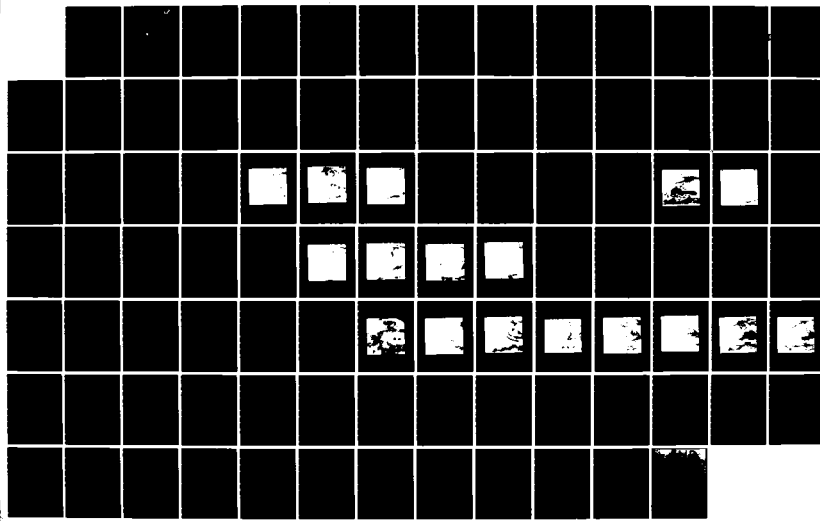
AD-A144 042 PREDICTABILITY OF INVERSIONS AT VANDENBERG (VBG) AFB
CALIFORNIA (U) NAVAL POSTGRADUATE SCHOOL MONTEREY CA
R B WILKERSON MAR 84

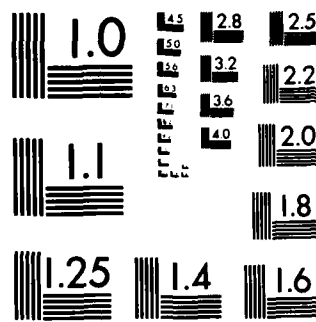
1/1

UNCLASSIFIED

F/G 4/2

NL





MICROCOPY RESOLUTION TEST CHART
NATIONAL BUREAU OF STANDARDS-1963-A

AD-A144 042

NAVAL POSTGRADUATE SCHOOL
Monterey, California



THESIS

DTIC
ELECTED
S D
AUG 7 1984
D

PREDICTABILITY OF INVERSIONS AT
VANDENBERG (VBG) AFB, CA.

by

Richard Boyd Wilkerson

March 1984

Thesis Advisor:

K. L. Davidson

Approved for public release; distribution unlimited.

84 08 06 030

SECURITY CLASSIFICATION OF THIS PAGE (When Data Entered)

DD FORM 1 JAN 73 1473 EDITION OF 1 NOV 68 IS OBSOLETE
S/N 0102-LF-014-6601

SECURITY CLASSIFICATION OF THIS PAGE (When Data Entered)

20. ABSTRACT (continuation).

obtained by vertical integration of the moisture budget equation (Q-method). Results of the model output were compared graphically and by use of RMS error statistics. These results were very poor and revealed that strong land influences on diurnal variations yield inversion height fluctuations which the model cannot reproduce. Further development of the model is necessary to overcome problems caused by the land influence.

Accession For		
NTIS GRA&I	<input checked="" type="checkbox"/>	
DTIC TAB	<input type="checkbox"/>	
Unannounced	<input type="checkbox"/>	
Justification		
By _____		
Distribution		
Available to Allies		
Approved and/or		
Dist	Final	
A/1		



S N 0102-LF-014-6601

Approved for public release; distribution unlimited.

Predictability of Inversions
at
Vandenberg (VFG) AFB, Ca.

by

Richard B. Wilkerson
Captain, United States Air Force
B. S., University of Utah, 1979

Submitted in partial fulfillment of the
requirements for the degree of

MASTER OF SCIENCE IN METEOROLOGY

from the

NAVAL POSTGRADUATE SCHOOL
March 1984

Author: _____



Approved by: _____



Thesis Advisor



Second Reader



Richard D. Munn
Chairman, Department of Meteorology

ABSTRACT

Accurate prediction of variations in the height of atmospheric inversions are required for optimum utilization of modern weaponry. A marine atmospheric boundary layer model was used to explore the influence of land on predictions of the inversion heights. Data for this evaluation were obtained from rawinsonde observations taken at Vandenberg AFB, California for each season. Vertical velocities for these data were obtained by vertical integration of the moisture budget equation (Q-method). Results of the model output were compared graphically and by use of RMS error statistics. These results were very poor and revealed that strong land influences on diurnal variations yield inversion height fluctuations which the model cannot reproduce. Further development of the model is necessary to overcome problems caused by the land influence.

TABLE OF CONTENTS

I.	INTRODUCTION	11
II.	MODEL DESCRIPTION	15
	A. BACKGROUND	15
	B. NPS MODEL PARTICULARS	17
	1. Atmospheric structure	18
	2. Dynamics within the mixed layer	18
	3. Radiative flux considerations	19
	C. MODEL APPLICATION	20
	1. Identify Synoptic Pattern	21
	2. Identify Initialization Parameters	21
III.	SYNOPTIC PATTERN DISCUSSION	24
	A. SUMMER CASE, PERIOD I (25-27 JULY 1977)	24
	E. WINTER CASE, PERIOD II (13-14 DECEMBER 1977)	33
	C. SPRING CASE, PERIOD III (13-16 APRIL 1981)	39
	D. FALL CASE, PERIOD IV (29 AUGUST - 5 SEPTEMBER 1981)	49
IV.	RESULTS	68
	A. DISCUSSION OF MODEL RESULTS FOR PERIOD I (SUMMER)	69
	E. DISCUSSION OF MODEL RESULTS FOR PERIOD II (WINTER)	74
	C. DISCUSSION OF MODEL RESULTS FOR PERIOD III (SPRING)	78
	D. DISCUSSION OF MODEL RESULTS FOR PERIOD IV (FALL)	80
	E. SUMMARY AND GENERAL COMMENTS	87

V. SUMMARY AND CONCLUSIONS	88
LIST OF REFERENCES	90
INITIAL DISTRIBUTION LIST	91

LIST OF TABLES

I.	Subsidence Rates for Model Runs	23
II.	July Inversion Results	69
III.	July Lifting Condensation Levels	69
IV.	July Potential Temperatures	70
V.	July Moisture Values	70
VI.	December Inversion Results	74
VII.	December Lifting Condensation Levels	75
VIII.	December Potential Temperatures	75
IX.	December Moisture Values	75
X.	April Inversion Results	78
XI.	April Lifting Condensation Levels	79
XII.	April Potential Temperatures	79
XIII.	April Moisture Values	80
XIV.	August-September Inversion Results	82
XV.	August-September Lifting Condensation Levels . . .	83
XVI.	August-September Potential Temperatures	84
XVII.	August-September Moisture Values	85

LIST OF FIGURES

3.17	Surface (a) and 500 mb (b) analyses 1200 GMT	
	16 April 1977	44
3.18	Satellite picture for 13 April 1981	45
3.19	Satellite picture for 14 April 1981	46
3.20	Satellite picture for 15 April 1981	47
3.21	Satellite picture for 16 April 1981	48
3.22	Rawinsonde example for Fall Case	51
3.23	Surface (a) and 500 mb (b) analyses 1200 GMT	
	29 August 1977	52
3.24	Surface (a) and 500 mb (b) analyses 1200 GMT	
	30 August 1977	53
3.25	Surface (a) and 500 mb (b) analyses 1200 GMT	
	31 August 1977	54
3.26	Surface (a) and 500 mb (b) analyses 1200 GMT	
	1 September 1977	55
3.27	Surface (a) and 500 mb (b) analyses 1200 GMT	
	2 September 1977	56
3.28	Surface (a) and 500 mb (b) analyses 1200 GMT	
	3 September 1977	57
3.29	Surface (a) and 500 mb (b) analyses 1200 GMT	
	4 September 1977	58
3.30	Surface (a) and 500 mb (b) analyses 1200 GMT	
	5 September 1977	59
3.31	Satellite picture for 29 August 1981	60
3.32	Satellite picture for 30 August 1981	61
3.33	Satellite picture for 31 August	62
3.34	Satellite picture for 1 September 1981	63
3.35	Satellite picture for 2 September 1981	64
3.36	Satellite picture for 3 September 1981	65
3.37	Satellite picture for 4 September 1981	66
3.38	Satellite picture for 5 September 1981	67
4.1	Graphical Depiction of Summer Case Observed and Forecasted Inversion Heights	73

4.2	Graphical Depiction of Winter Case Observed and Forecasted Inversion Heights	77
4.3	Graphical Depiction of Spring Case Observed and Forecasted Inversion Heights	81
4.4	Graphical Depiction of Fall Case Observed and Forecasted Inversion Heights	86

I. INTRODUCTION

Historically, advanced detection and surprise attacks have been an area of interest to the military community. Knowledge about the effects of atmospheric boundary layer (ABL) inversions on electromagnetic signals is well known and documented. Advance knowledge of inversion changes can have a direct effect on military planning conducted by all services.

With technological advances, our weaponry has become highly sophisticated (e.g., the development of "smart" bombs) and dependent on electromagnetic propagation for guidance control. The guidance components for these weapons depend on many different wavelengths, ranging from the visible to the microwave, dependent on the specific use of the weapon. The weapons depend on the transmission and reception of these signals to locate and follow targets. Difficulties arise when atmospheric conditions are such that signal performance is distorted by refraction. Only those areas which affect propagation of radar signals will be discussed in this thesis. Other propagation types, such as optical, and the atmospheric parameters affecting them will not be addressed.

Signal propagation is dependent on the index of refraction which is a function of temperature and humidity. Refraction of a signal occurs as that signal moves through vertical gradients of temperature and humidity. Atmospheric conditions which enhance refraction are inversions, which cause strong gradients of temperature and humidity, or rapid changes of humidity near the surface. Occurrence, height and intensity of inversions are strongly dependent on local and synoptic atmospheric conditions. The importance of

predicting propagation is obvious but to do so with accuracy first requires accurate prediction of the meteorological parameters affecting it. Of obvious importance is the prediction of changes in the temperature and humidity profiles, both of which are highly variable and can completely change their vertical profile within a matter of hours. Other parameters such as vertical velocity and surface wind speeds will be discussed later.

The ability to forecast inversions and how they may vary directly influences the effectiveness of modern weaponry. It is readily apparent that improvements in this forecasting ability is of paramount importance in making military plans which involve choosing the type weapon best suited for a particular mission. As long as there are functions dependent on signal transmissions there will remain a need to increase the ability to forecast the atmospheric parameters which contribute to propagation.

The model used to investigate inversion heights is a marine atmospheric boundary layer (MABL) model which has been modified for use at the Naval Postgraduate School (NPS). The factors incorporated into this model include potential temperature and specific humidity within the well-mixed region and their gradients at the base of the inversion. Use of these parameters make this model applicable to studying inversion changes. Actual discussion of the model will be provided in Chapter II.

Another area where advance knowledge of ABL inversion changes would be useful is in single-station forecasting. The effects of changes in the inversion are found not only to effect electronic transmissions but also to indicate possible changes to current weather conditions. Therefore, any improvements in our ability to predict these changes will be important to land-based and sea-based operations, since improvement in this area of prediction also will be reflected in the daily weather forecast.

This thesis completes an analysis on four time periods of data obtained from Vandenberg AFB, California. These data periods each cover a different season and vary from two to eight days in length. In conducting this examination vertical velocities for Vandenberg AFB were calculated from their rawinsonde data. Each days data were run through the NPS MABL prediction model to establish the forecast trend for that period. Results from the model's forecasts were compared to data from later reports for correlation and to determine accuracy of the model. Successive runs of the model were made until each data set has been completed and determination as to how well the model predicts inversion heights in each 24 hour forecast.

One of the time periods of data chosen for study is, by choice, coincident with a data period used by Gleason (1982). His study was directed at effectiveness of the model for more of a pure marine location and for this reason data from San Nicolas Island was chosen. This study uses data from Vandenberg AFB since it is a coastal station and will have somewhat different surface conditions due to the continental influence. See Fig. 1.1 for a geographical orientation of the area of interest. Once the Vandenberg AFB data had been studied, the San Nicolas Island results were used to make comparisons. The results of this comparison are of interest since they will indicate whether or not there are potential problem with the MABL model when used in a regime strongly influenced by land as compared to a regime closely resembling marine conditions.

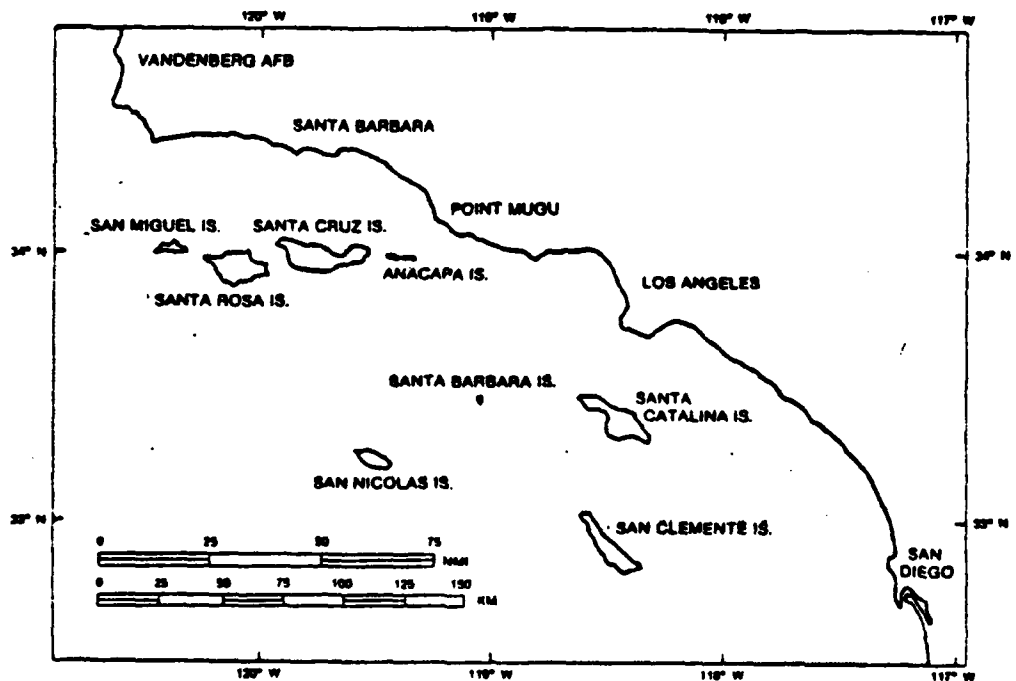


Figure 1.1 Southern California Coastal Regions.

II. MODEL DESCRIPTION

A. BACKGROUND

The MABL model in use at the Naval Postgraduate School (NPS) is a zero-order, two layer, integrated mixed layer model (Davidson et al. 1984). This is a modified version of the model developed by Stage and Businger (1981). The two layers consist of the well-mixed, turbulent boundary layer and the relatively non-turbulent free atmosphere. Separating these layers is the transition zone known as the inversion. The term, "zero-order", applies to this model because the inversion is considered a jump from one value to another instead of having a finite gradient. Thus, we assume that, at the inversion, the equivalent potential temperature (θ_e), and the total specific humidity (q_t) undergo zero-thickness jumps.

Total specific humidity and equivalent potential temperature are conserved quantities in pseudo-adiabatic processes and, for this reason, are assumed well-mixed within the boundary layer. They are given by:

$$q_t = q_v + q_l \quad (2.1)$$

where q_v is the water vapor mixing ratio and q_l is the liquid water mixing ratio; and

$$\theta_e = \theta + L_v / (C_p q_v) \quad (2.2)$$

where θ is the potential temperature, L_v is the latent heat for vaporization of water, and C_p is the specific heat at constant pressure of air. A third fundamental dependent

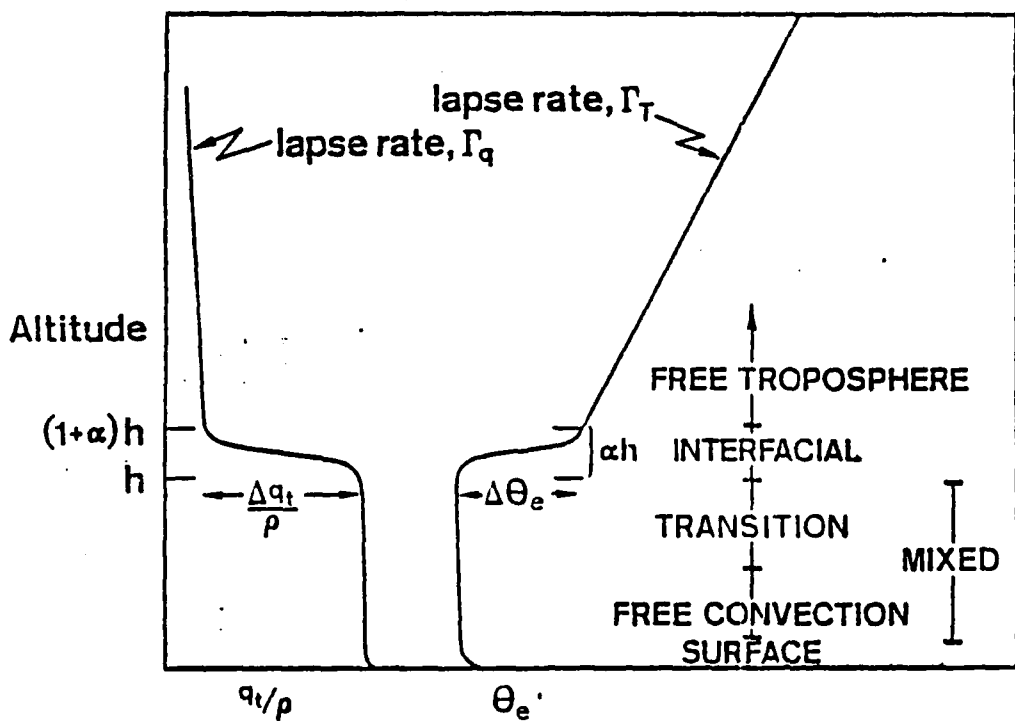


Figure 2.1 Typical potential temperature and moisture profiles.

variable is the mean mixed layer depth (h). Typical profiles of these parameters are shown in Fig. 2.1. As can be seen in Fig. 2.1, both θ_e and q_t are assumed to have constant values throughout the mixed layer. Above this is the interfacial region, or inversion, where the jump occurs.

One of the more appealing features about this model is that it runs from input parameters gleaned from routine meteorological and oceanographic data. These parameters are: surface layer humidity, temperature and winds, vertical gradients of temperature and humidity above the

mixed layer, and sea-surface temperature (SST). Readily available rawinsonde observations can be used to determine all input parameters except SST. SST values can be obtained from satellite interpretation or direct measurements.

The predictive equations for the three dependent variables are given by:

$$\begin{aligned} \frac{dq_t}{dt} &= h^{-1} ((w'q'_t)_0 + w_e \Delta q_t) \\ \frac{d\theta_e}{dt} &= h^{-1} ((w'\theta'_e)_0 + R_c - R_B + w_e \Delta \theta_e) \quad (2.3) \\ \frac{dh}{dt} &= w_D + w_e \end{aligned}$$

where d/dt represents the time rate of change of the variable following a column of air. $(w'\theta'_e)_0$ and $(w'q'_t)_0$ are the surface turbulent fluxes of θ_e and q_t , while the Δ terms are the magnitude of the jumps at the inversion. Other quantities introduced here are: 1) w_e - the entrainment rate; 2) w_D - the large-scale vertical velocity at the inversion height (initialized using the subsidence rates described later in this chapter); 3) R_B - the rate of radiative heat loss per unit area near the cloud top; and 4) R_c - the rate of radiative heat gain per unit area at the cloud base. (Haggerty, 1983)

B. NPS MODEL PARTICULARS

The use of a well-mixed layer, along with other developments, made modifications to the model described by Stage and Eisinger (1981) necessary. The NPS integrated MABL differs from others in the specifics of surface flux, radiative flux and the zero gradient assumption. The following discussions are brief since the references (Davidson et al. 1984) are quite complete.

1. Atmospheric structure

The profile of a well-mixed atmospheric variable, ϕ , is represented as

$$\begin{aligned}\phi(z) &= \phi_{ms} + \Gamma_{\phi m} z & z \leq h \\ \phi(z) &= \phi_{mh} + \Gamma_{\phi} (z-h) & z > h\end{aligned}\quad (2.4)$$

where m refers to the mixed layer, s to the surface value, h is the height of the mixed layer, z is the height, $\Delta\phi$ is the jump in ϕ across the inversion zone, Γ_{ϕ} is the gradient above the inversion, and $\Gamma_{\phi m}$ is the gradient in the mixed layer (assumed to be zero).

2. Dynamics within the mixed layer

The model predicts the time evolution of the mixed layer values of q_t , θ_e , and h (see Eqn. 2.3). At initialization, the lapse rates for these quantities are held constant while larger, synoptic scale observations provide the input values of the boundary layer wind for the entire forecast period.

Surface fluxes of sensible heat and water vapor are determined through an application of the bulk aerodynamic formula (Davidson et al. 1978). These fluxes are driven by the bulk air/sea differences and are expressed as

$$\begin{aligned}(w'\theta'_e)_0 &= C_{\theta}^{1/2} (\theta_0 - \theta_m) u_* \\ (w'q'_t)_0 &= C_{\theta}^{1/2} (q_0 - q_m) u_*\end{aligned}\quad (2.5)$$

where C_{θ} is the ten meter, stability dependent, drag coefficient, u_* is the friction velocity, and θ_0 and q_0 are the respective sea-surface values.

Parameterization for the entrainment rate is that given by Stage and Businger (1981). This parameterization allows closure of the system of equations and determines the time evolution of the inversion height. It also brings the turbulent kinetic energy (TKE) budget into the formulation since entrainment of heat flux across the stable inversion requires TKE, that is, work is done by this process. Here the assumption used for closure states that the dissipation rate of TKE is a fixed fraction ($1-\Lambda$) of the production rate, where Λ is the entrainment coefficient, set equal to 0.2. Within the TKE equation are terms which provide for production and dissipation, therefore it is assumed that both occur within the mixed layer, rather than only where there is negative buoyancy flux. These are associated through the use of the turbulent scaling velocity for the mixed layer, w_* , and the mixed layer depth (h) for the scaling length.

3. Radiative flux considerations

When considering radiation flux and its effects on the mixed layer there are several points which must be understood. Distinction must be made between long-wave fluxes for clear or cloudy cases, and short-wave fluxes.

a. Long-wave radiative flux

Under cloudless sky conditions, the net long-wave radiative flux is determined using the water vapor and temperature profiles. The flux is calculated by integrating, from the surface ($Z=0$) to the top of the mixed layer ($Z=h$), the flux emissivity profile where the emissivity is determined from the Stefan-Boltzmann law (Fleagle and Businger 1980). The aforementioned modification has also been applied.

The presence of clouds necessitates the calculation of the net radiative flux at both the cloud top and the cloud base. These calculations are also made using the Stefan-Boltzmann law. When the cloud top flux is being determined, the input temperatures are the cloud top temperature and the effective radiative sky temperature. For the cloud base the input temperatures are the temperatures at the cloud base and at the sea surface. It is also important to note that, in this case, the flux divergence between the sea surface and the cloud base is neglected.

b. Short-wave radiative flux

The MABL model calculations of short-wave radiation take into consideration both direct and diffuse components. Both scattering and absorption contribute to short-wave extinction. The scattering contribution to the short-wave radiative flux is determined through use of the delta-Eddington method, where the mixed layer scattering is due to atmospheric particles, cloud droplets in the cloudy case and sea-salt aerosols in the clear sky case. Absorption is primarily the result of water vapor and is taken into account when the incident flux at the top of the mixed layer is determined.

C. MODEL APPLICATION

All model runs for this thesis were done such that the situation approximated to a real forecast run. That is, the model was initially set to run with a single sounding and an estimate of -0.0005 m/s for the subsidence. Further runs were made as each new sounding could be added. This presents a realistic representation of what one could expect from the model for the Vandenberg AFB area.

Preparation for running the model requires that several points or items be considered. These consist of identifying the synoptic pattern and initialization parameters; will be discussed below.

1. Identify Synoptic Pattern

Before checking on input data for the model the overall synoptic pattern must be checked. To do this one utilizes all available meteorological data (e.g., surface and upper air synoptic analyses, as well as satellite, rawinsonde and individual surface observations). The desired synoptic situation for optimum model predictability is to have the area of interest dominated by a high pressure system.

2. Identify Initialization Parameters

The next step in preparing to make the model runs is to determine the input parameters. Potential temperature and moisture values for the mixed layer, height and strength of the jump, surface wind, sea-surface temperature, vertical velocity and the lapse rate above the jump are the necessary parameters and, of these, a good determination of the jump value across the inversion is critical.

Except for vertical velocities, parameters are determined from the vertical soundings, and can be done manually or through the use of a digitizing program. A sample of a digitized rawinsonde appears in Fig. 2.2. Extreme care must be used so that the values determined represent the true sounding or serious error can result.

The vertical velocity or, in our case, the subsidence rate for the forecast start time must be determined. There are several means for calculating vertical velocity but none, to date, provide the accuracy desired. With this in mind, the method which has proved to be most accurate was

used. This method is the Q-method which is an expression for vertical velocity derived from the vertical integration of the moisture budget equation and is given by:

$$w = \frac{\Delta(q+1)(dh/dt) - h(d(q+1)/dt) + (w'q')_0}{\Delta(q+1) + \beta(h/2)} \quad (2.6)$$

where q and l are vapor and liquid water contents, and β , their vertical gradient (Gleason, 1982). The computer program used to calculate the vertical velocity uses current data as well as data within the previous 24 hours. The use of previous rawinsonde data is allowed since the Q-method equation includes total change with respect to time (d/dt) for the inversion height and the total moisture. The vertical velocities output from the program are for each data period input. These values are then averaged to get

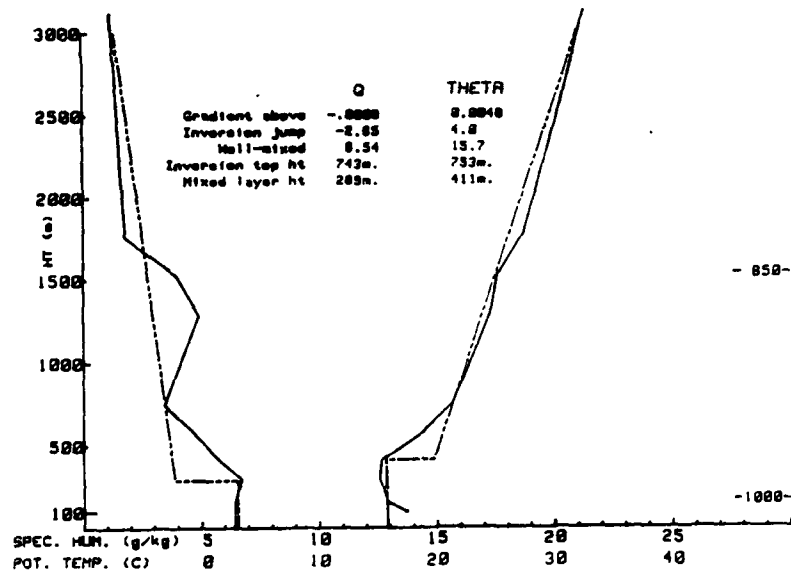


Figure 2.2 Sample of digitized rawinsonde.

the date for the entire period with the final subsidence rate calculated being the one used in the model. The only difficulty encountered with this method was when the subsidence inversion height was increasing at a rate sufficient to yield a positive average. When this occurred the model input rate was set to zero. Table I gives the subsidence rates (m/s) used for the model runs.

TABLE I
Subsidence Rates for Model Runs

DATE	GMT	SUBSIDENCE	DATE	GMT	SUBSIDENCE
July 25	00	-0.005	August 29	00	-0.005
	12	-0.003948		12	-0.0008393
	00	-0.003359		00	0.00
	12	-0.0008265		12	-0.0002389
	00	-0.01489		00	-0.0004126
	12	-0.001553		12	0.0
	00	-0.002856		00	0.0
				2	-0.005934
				12	-0.001676
				00	0.0
December 13	00	-0.005	September 1	00	-0.000082
	12	-0.005813		12	0.0
	00	-0.002856		00	-0.0006649
	12	0.0		12	-0.0002713
				00	-0.0005856
April 13	00	-0.005	September 2	00	-0.001524
	12	-0.002019		12	0.0
	00	0.0		00	0.0
	12	-0.0003651		12	-0.0002713
	00	0.0		00	-0.0005856
	12	0.0		12	-0.001524
14	00	-0.002208		00	0.0
	12	-0.002988		12	0.0

III. SYNOPTIC PATTERN DISCUSSION

Four data sets were used for evaluation of model validity. These sets include a summer period (25 through 27 July 1977), a winter period (13 and 14 December 1977), a spring period (13 through 17 April 1981), and a fall period (29 Aug through 5 September 1981). Large scale analyses were for as close to 1200 Greenwich Mean Time (GMT) as possible. In most cases the satellite pictures will be at 1745 GMT since these pictures best display the area of interest.

This discussion will be of the overall weather picture for the eastern North Pacific Ocean and the western United States. Included will be conditions over the area as a whole and unique or differing conditions at Vandenberg AFB itself. Satellite pictures, surface weather analyses, and upper air analyses (500 millibars) will be used to determine the synoptic situation of each period.

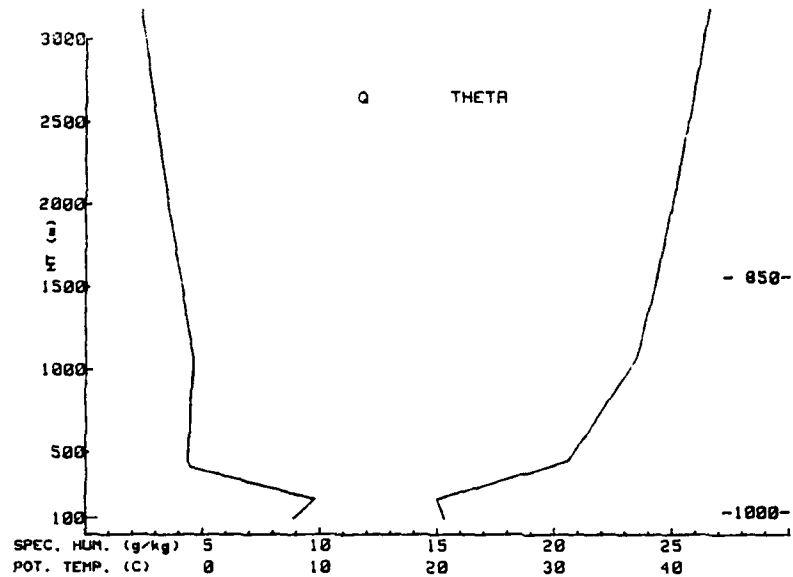
A. SUMMER CASE, PERIOD I (25-27 JULY 1977)

The surface and 500 millibar (mb) synoptic patterns for this period appear in Figs. 3.2 through 3.4. During this period the coastal region was dominated by a high pressure system over the North Pacific Ocean with the thermal troughing extending from Mexico northward into the high desert region of Arizona and southeastern California. Such a synoptic pattern usually produces weak onshore flow along the southern California coastal regions. The upper air analyses (500 mb) showed no strong westerly flow over California during the entire period.

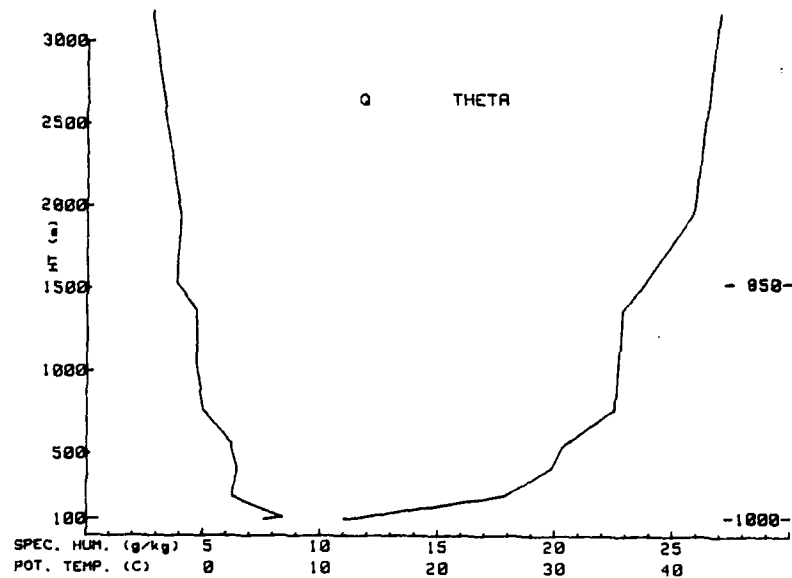
During this period the Pacific high pressure system moved northeastward and on 27 July, weakened as a stationary front developed off the northwest coast. Also of importance on 27 July was the development of a low pressure center west of Los Angeles, California. Even with this development the precipitate flow remained onshore in the Vandenberg AFB region.

The rawinsonde data revealed a subsidence type inversion throughout the period, see Fig. 3.1. There was also a diurnal variation in the inversion base. Each day the base ranged from the surface at 1200 GMT to a height above 650 feet at 0000 GMT. An example of this diurnal change also appears in Fig. 3.1.

The satellite pictures for this period appear in Figs. 3.5 through 3.7. Only patchy areas of low clouds along the California coast appear on the satellite pictures. These areas were in the San Francisco bay area and the coastline south of Los Angeles. The only other area of low clouds was two to three degrees longitude west of Vandenberg AFB. There was no significant changes to the coastal locations of the low clouds while the area over the water had some dissipation and was even further offshore. The Vandenberg AFB vicinity remained under clear skies during the entire period.

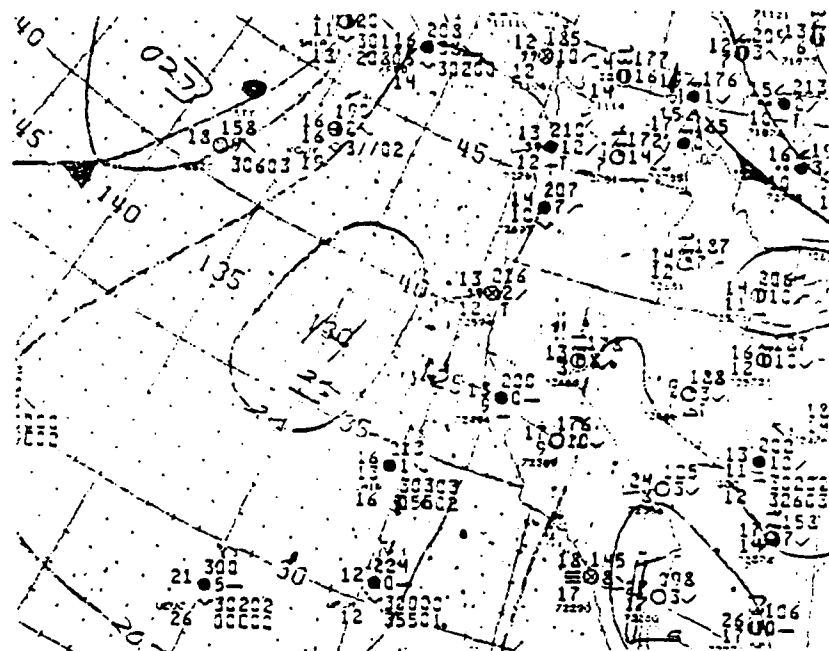


(a) 0000 GMT Sounding

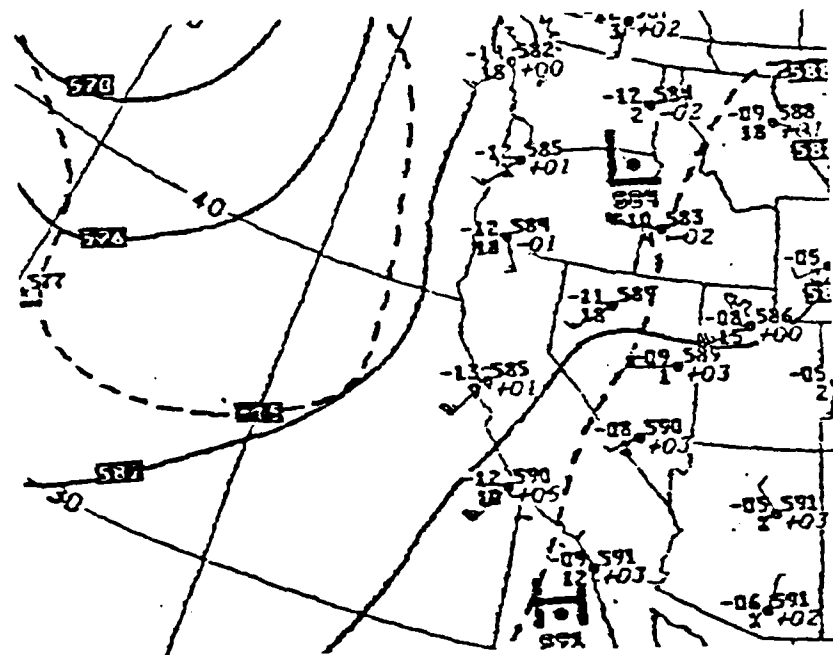


(b) 1200 GMT Sounding

Figure 3.1 Example of Summer Case rawinsonde and diurnal change in inversion.

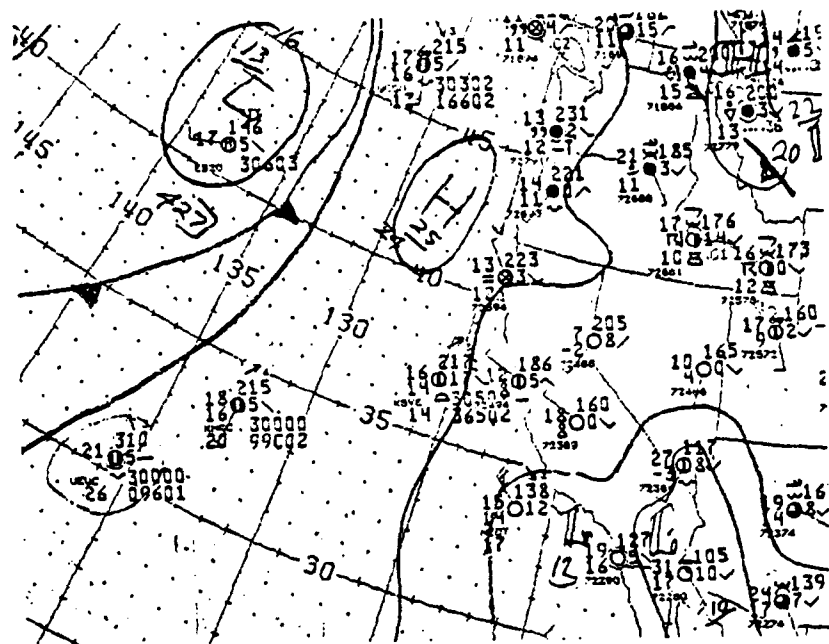


(a)

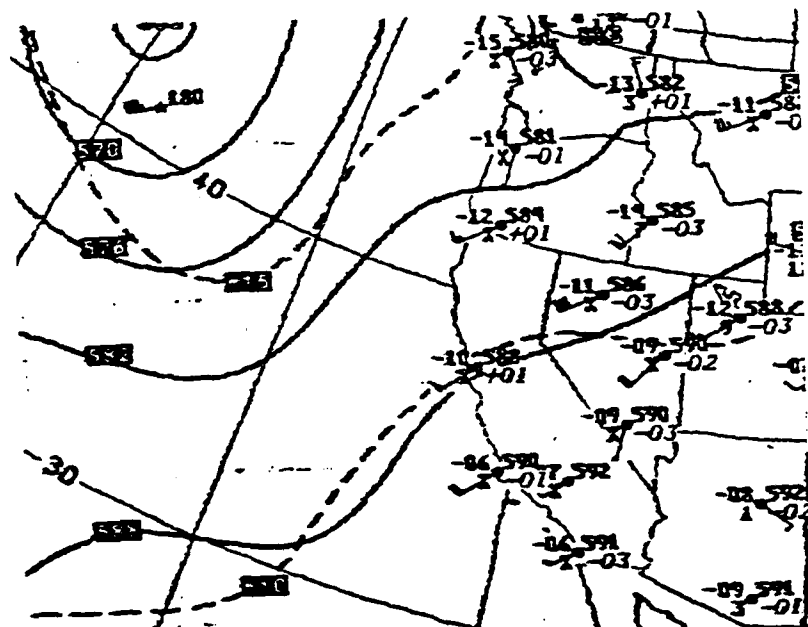


(b)

Figure 3.2 Surface (a) and 500 mb (b) analyses
1200 GMT 25 July 1977.

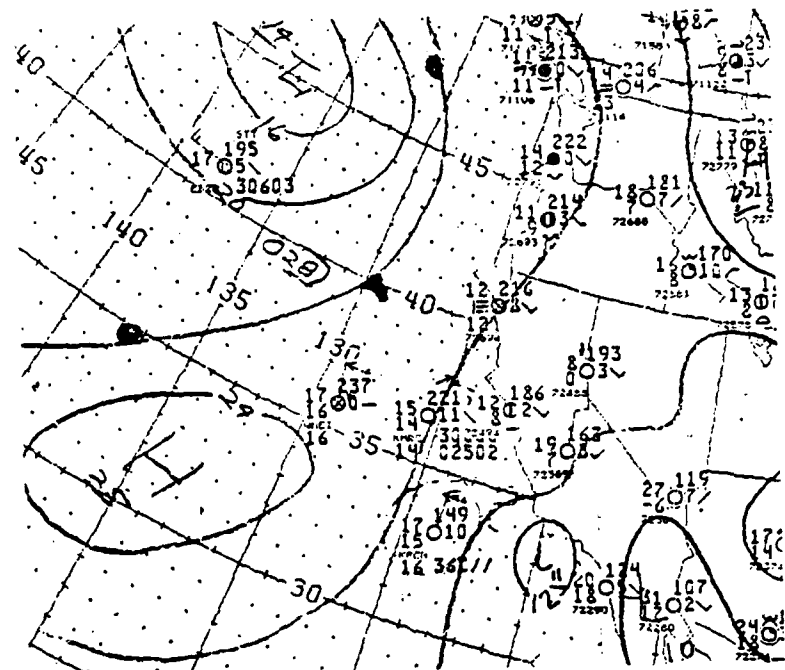


(a)

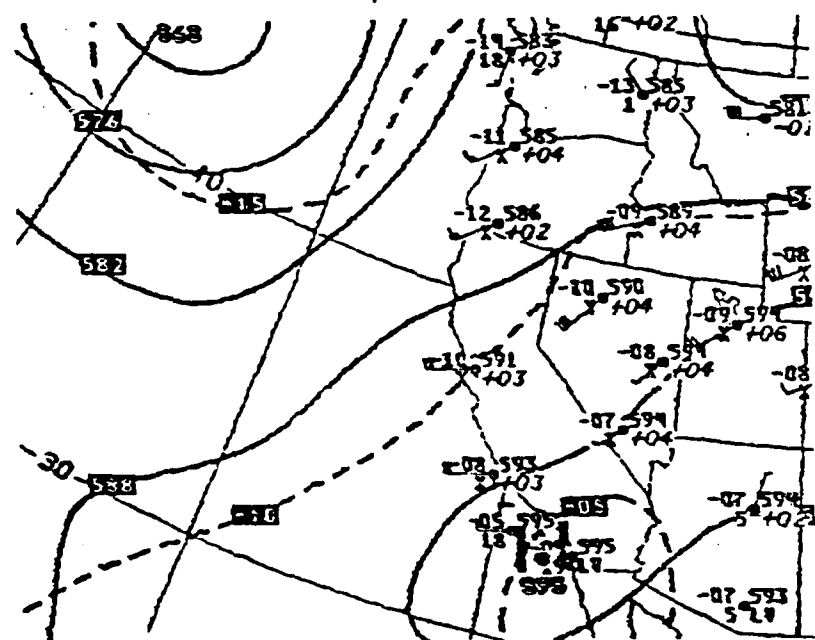


(b)

Figure 3.3 Surface (a) and 500 mb (b) analyses
 1200 GMT 26 July 1977.



(a)



(b)

Figure 3.4 Surface (a) and 500 mb (b) analyses
 1200 GMT 27 July 1977.

1745 25JL77 32A-1 00781 15871 WB2

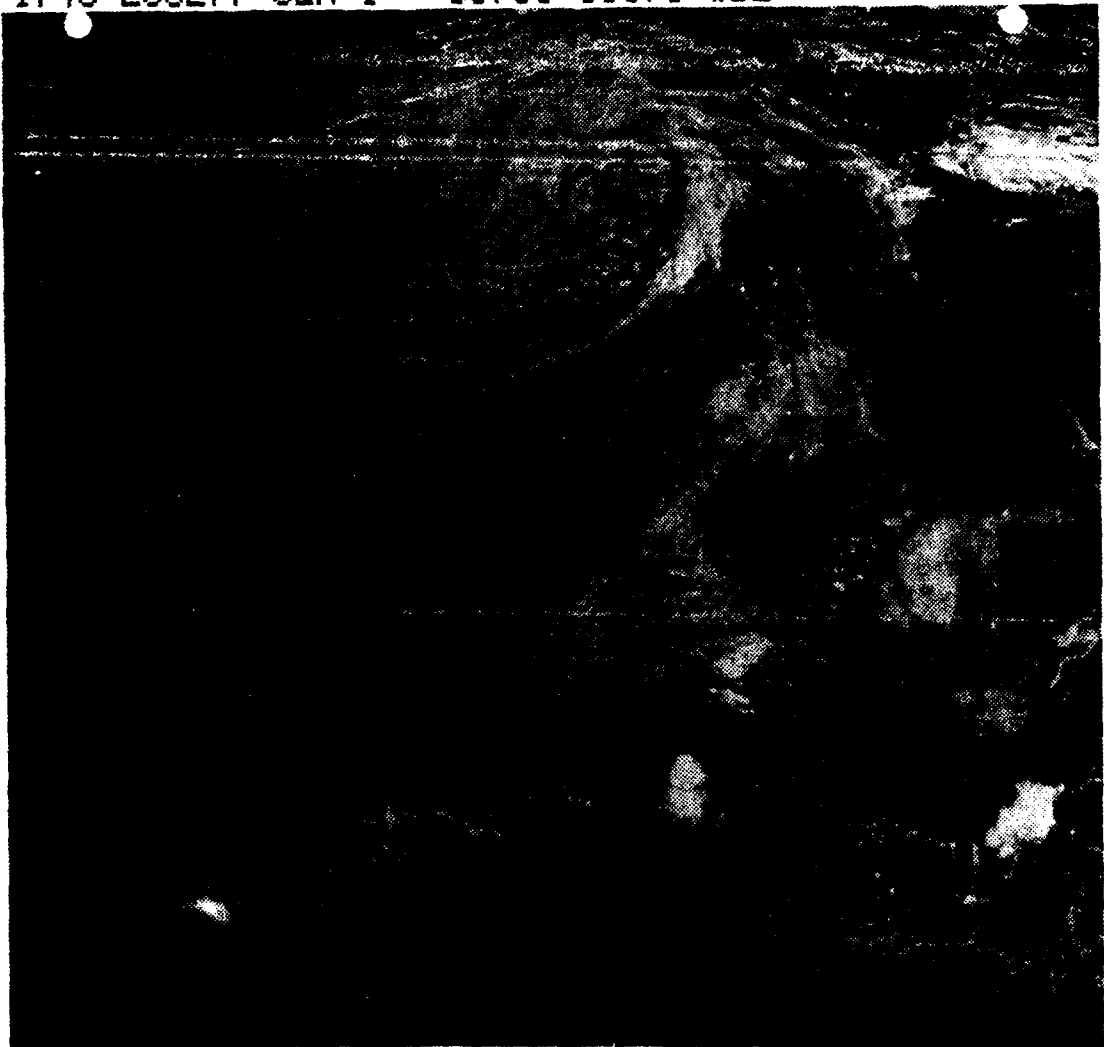


Figure 3.5 Satellite picture for 25 July 1977.

1745 26JL77 32A-1 00751 15871 WB2

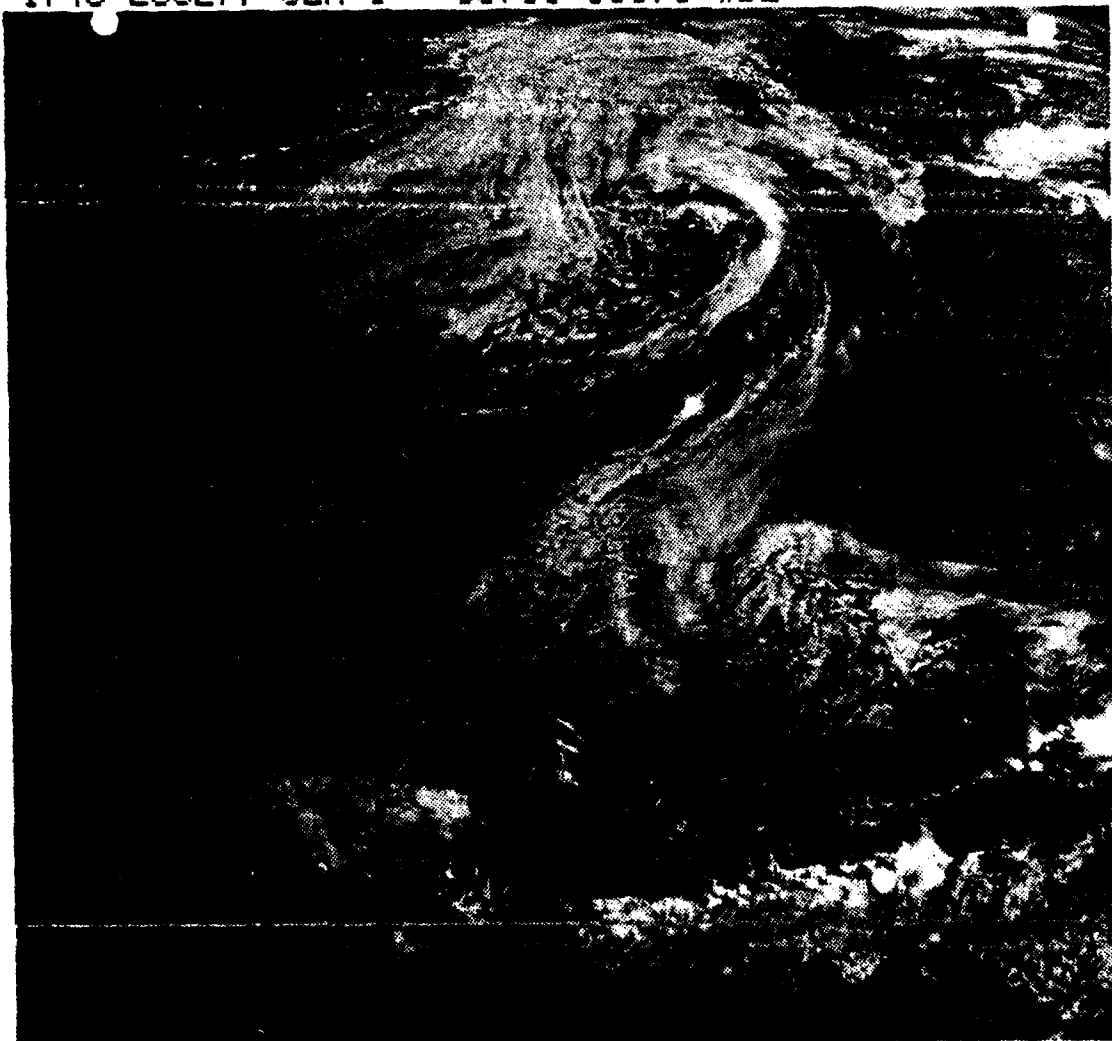


Figure 3.6 Satellite picture for 26 July 1977.

1745 27JL77 32A-1 00841 15871 WB2

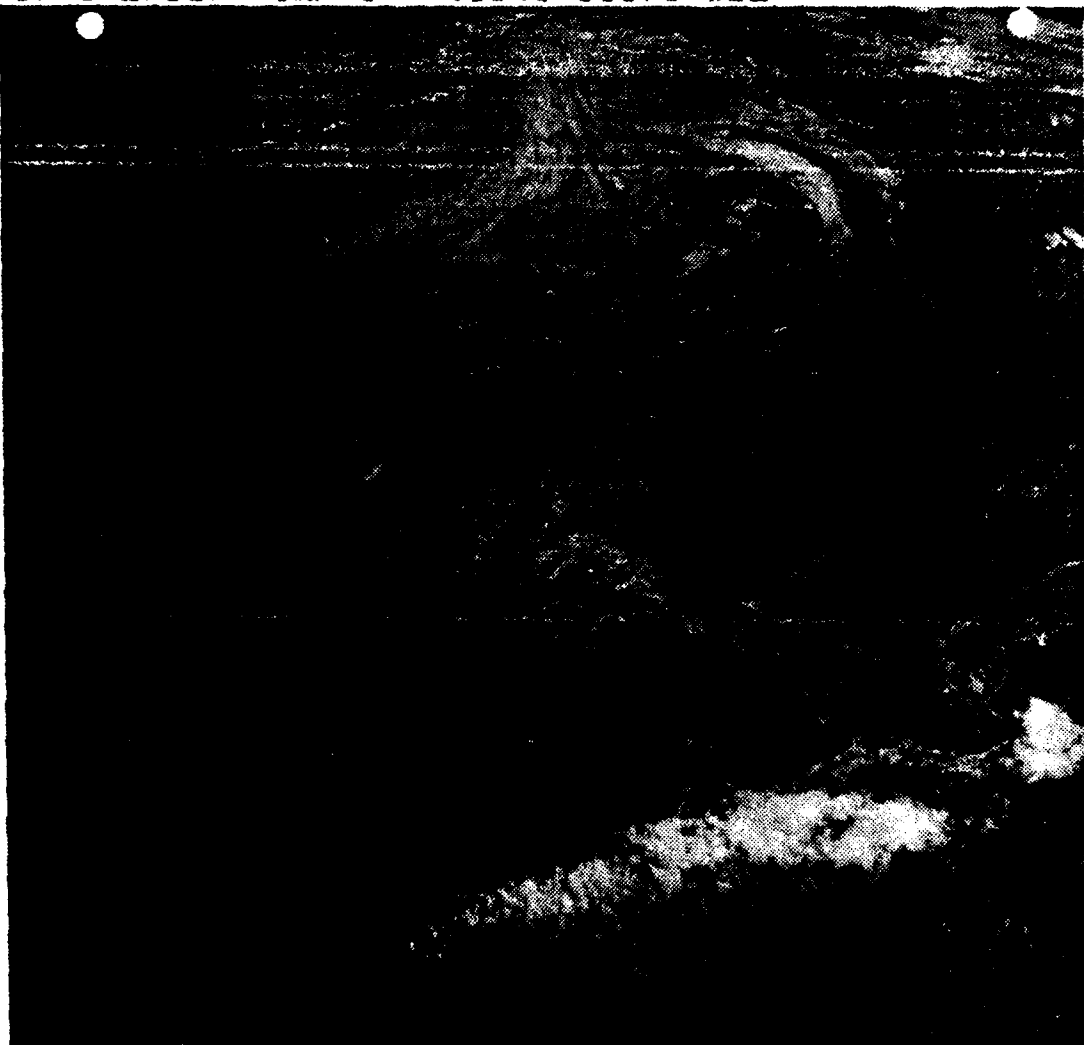


Figure 3.7 Satellite picture for 27 July 1977.

E. WINTER CASE, PERIOD II (13-14 DECEMBER 1977)

The general surface and 500 mb analyses appear in figures 3.9 and 3.10. A difference between this synoptic pattern and that found in the other periods is in this pattern the desired onshore flow exists but it does not arise from the strong Pacific high and thermal troughing but from a high pressure cell that had separated from the main Pacific cell and moved in over central California. The strongest westerly flow aloft was found to the north of California with the Polar jet moving across the Washington - Oregon region. Westerly flow over Vandenberg AFB was stronger than in other periods.

The primary aspect is that on 13 December a high pressure center moved over central California with the large high pressure system still maintained over the North Pacific Ocean. Weak thermal troughing was also extending northward into California. The overall result of these surface patterns was weak onshore flow in the Vandenberg AFB and San Nicolas Island regions. The only other significant feature in the 13 December analysis was the frontal system moving into the Pacific Northwest.

On 14 December the high pressure center dissipated leaving the Pacific high pressure system and ridging across central California. Weak thermal troughing continued in the southern California area. Offshore flow also continued to dominate the southern California coastline. The frontal system from the 13th moved eastward and a trailing warm front moved to northern California.

Fig. 3.8 is an example of the vertical soundings for this period. The rawinsonde data showed subsidence type inversions on both days. Most important is that on 13 December at 0000 GMT the inversion was very weak and not well structured. The inversion strengthened and remained

aloft until 1200 GMT on 14 December when it was observed as a surface based inversion. At this time the inversion reached the maximum strength for the period.

The satellite pictures for this period appear in Figs. 3.11 and 3.12. Clear skies in the Vandenberg AFB area with a frontal system moving into the northern California regions appear in the satellite picture for 13 December. There is very little indication of low clouds along the southern California coastline. By 14 December the front is well into northern California with increased cloudiness across central California. There has also been an increase in the amount of low clouds along the southern California coast. Patchy stratus follows the coast south of Los Angeles and a large area now sits off the Vandenberg AFB coast.

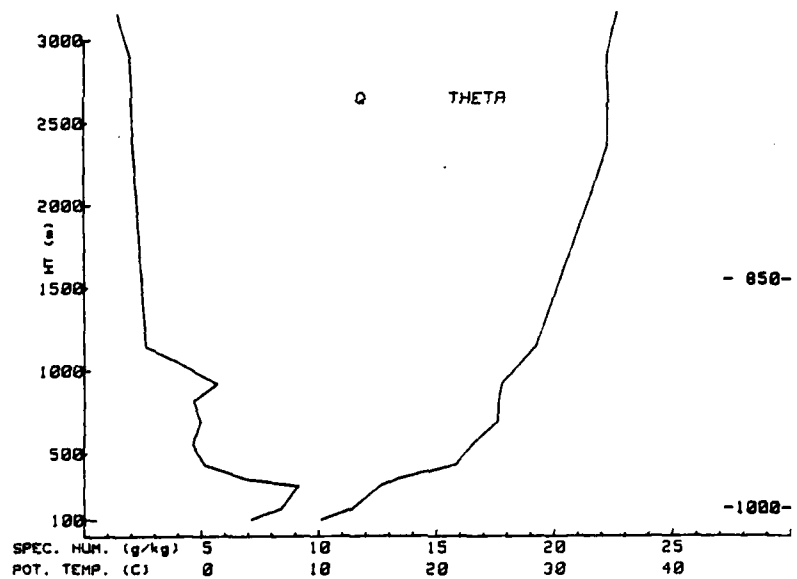
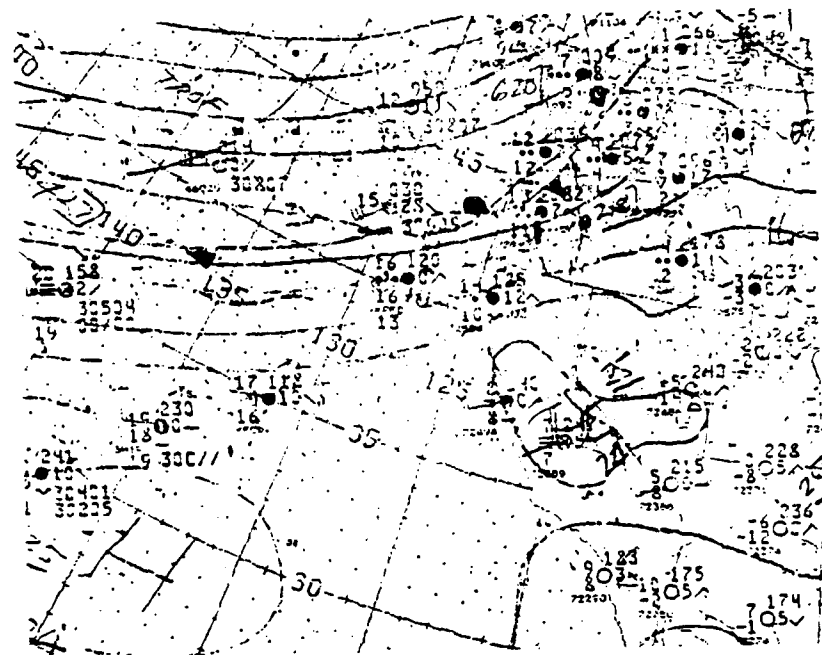
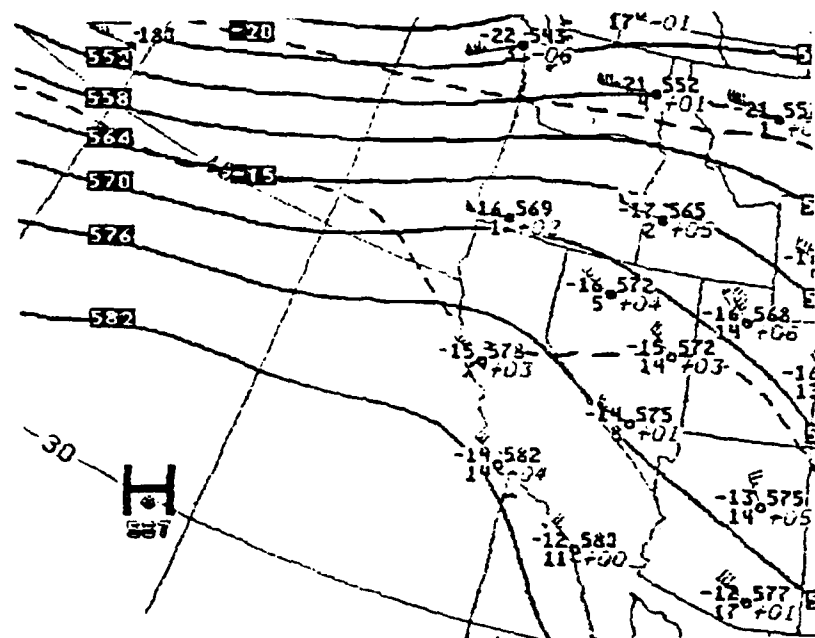


Figure 3.8 Example of Winter Case rawinsonde.

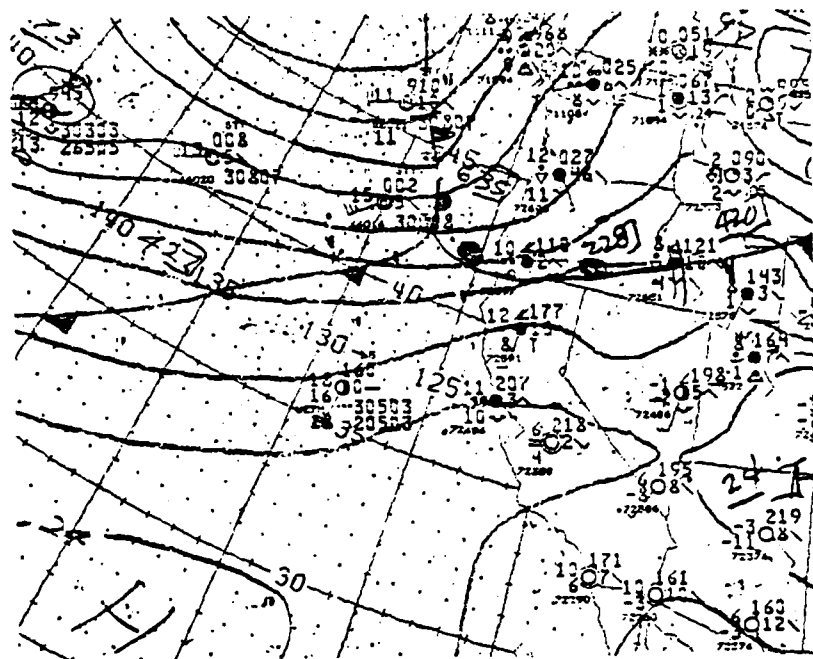


(a)

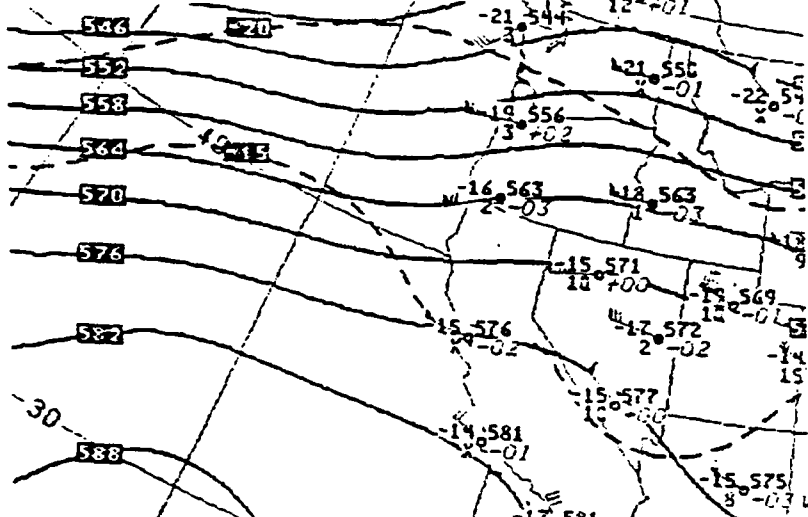


(b)

Figure 3.9 Surface (a) and 500 mb (b) analyses
1200 GMT 13 December 1977.



(a)



(b)

Figure 3.10 Surface (a) and 500 mb (b) analyses
1200 GMT 14 December 1977.

1815 13DE77 32A-2 00341 19211 UC2

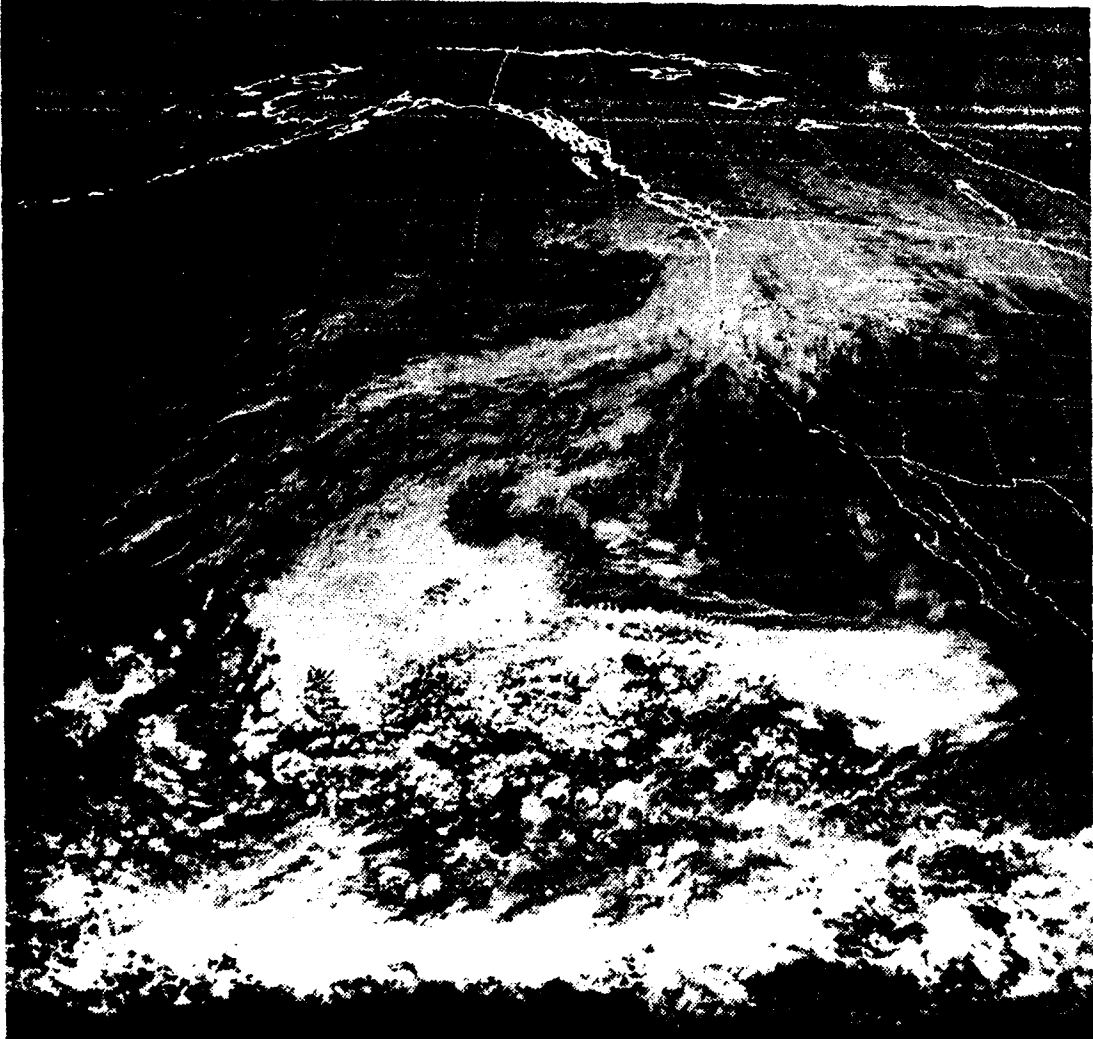


Figure 3.11 Satellite picture for 13 December 1977.

1745 14DE77 32A-1 00231 16051 WB2



Figure 3.12 Satellite picture for 14 December 1977.

C. SPRING CASE, PERIOD III (13-16 APRIL 1981)

The synoptic patterns for this period appear in Figs. 3.14 through 3.17. The dominating feature was a high pressure system extending northeastward from the North Pacific Ocean regions across Washington into Canada. Thermal troughing dominated the high desert regions of California and extended into northern California. The predominate southern California coastal flow, generated by these patterns, was onshore. 500 mb analyses show light and variable winds with tendencies toward formation of a low pressure center through the period. The strongest westerly flow remained well north of the Vandenberg AFB area.

On 13 April the Pacific high was strong but showing a tendency to weaken as the longwave pattern extended into Canada. As the longwave high pattern shifted to the central United States the Pacific high weakened. The thermal trough in southern California continued to dominate but also had some weakening.

By 15 April the Pacific high system had begun to strengthen with some ridging across central California. The high continued intensification through the remainder of the period. On 16 April the ridging extended into the Washington area with the Pacific high pressure center beginning to move northeastward. Throughout this portion of the period the thermal trough showed very little variation. The only other key occurrence from the 15th to the 16th was the movement of a cold front across the Pacific Northwest into Nevada.

Fig. 3.13 is an example of the rawinsonde soundings for this period. Rawinsonde reports during this period had subsidence inversions with much daily variation. At the beginning of the period the inversion was weak and aloft. Diurnal variations intensified the inversion but also

brought it to the surface. This pattern continued through the 14th but on the 15th the inversion intensified at 0000 GMT and remained aloft until 1200 GMT on the 16th. During the latter half of the period there was some fluctuation in the intensity but over all the inversion remained strong.

These satellite pictures appear in Figs. 3.18 through 3.21. On 13 April the satellite showed Vandenberg AFB under clear skies while the coastal region south of there was dominated by low clouds. By 14 April the area of coverage by low clouds increased and Vandenberg AFB was within that area. Low clouds continued to dominate the Vandenberg AFB area with some dissipation beginning on 15 April. 16 Apr showed only thin coverage of low clouds over the Vandenberg AFB area with the denser coverage south of the area.

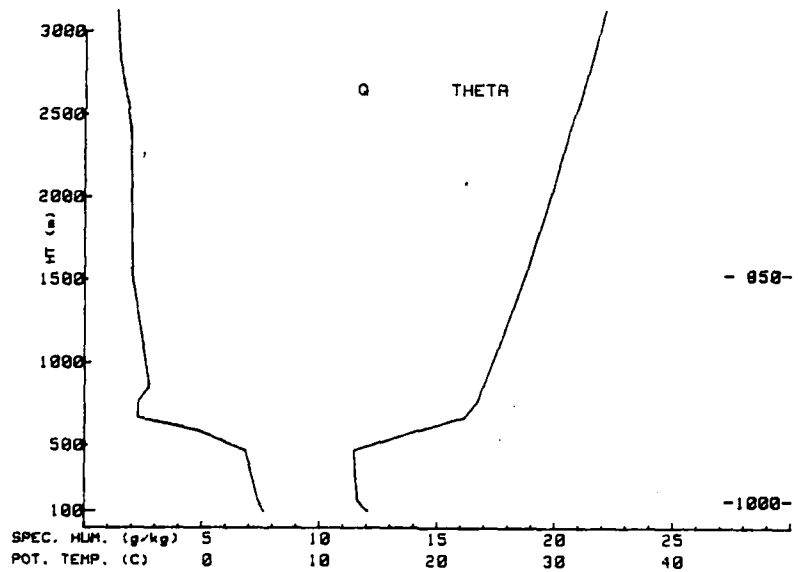
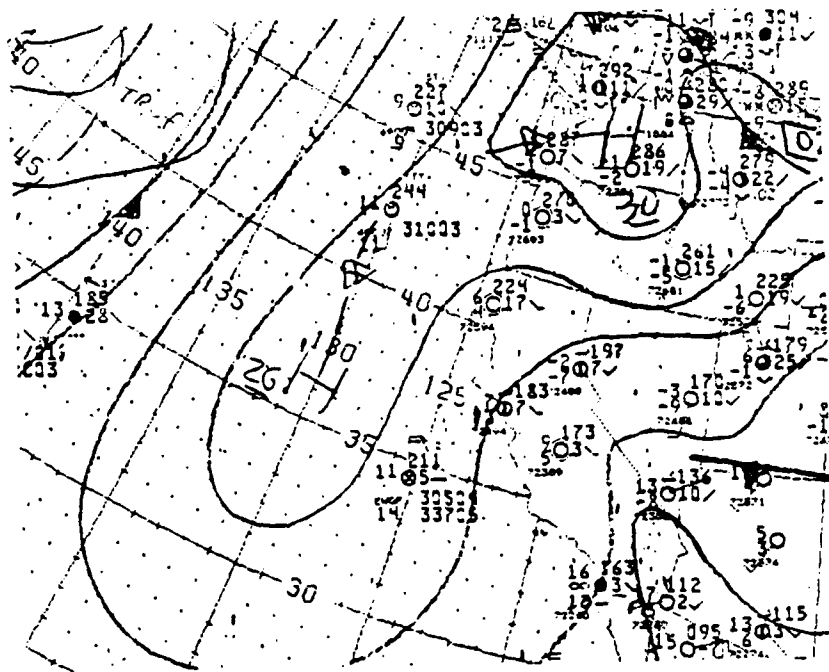
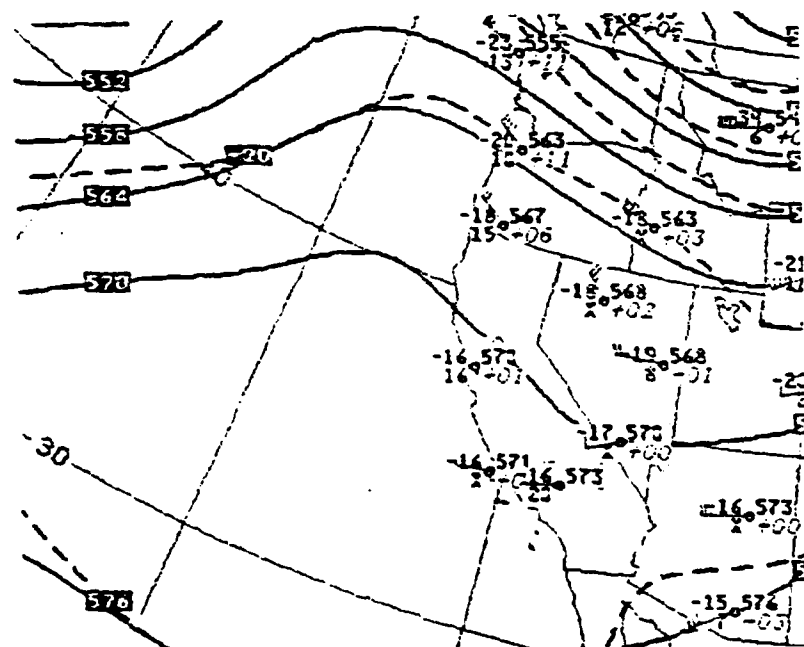


Figure 3.13 Example of rawinsonde for Spring Case.

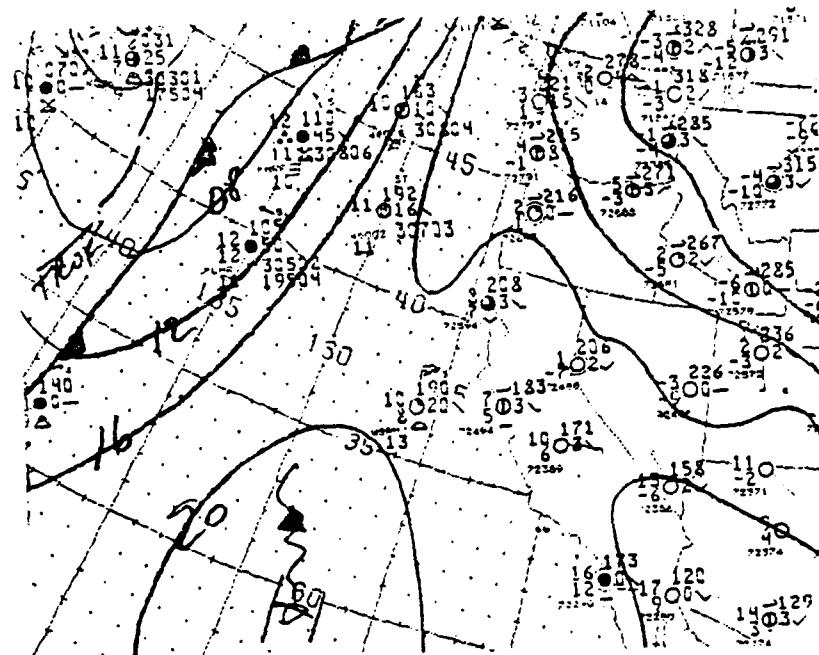


(a)

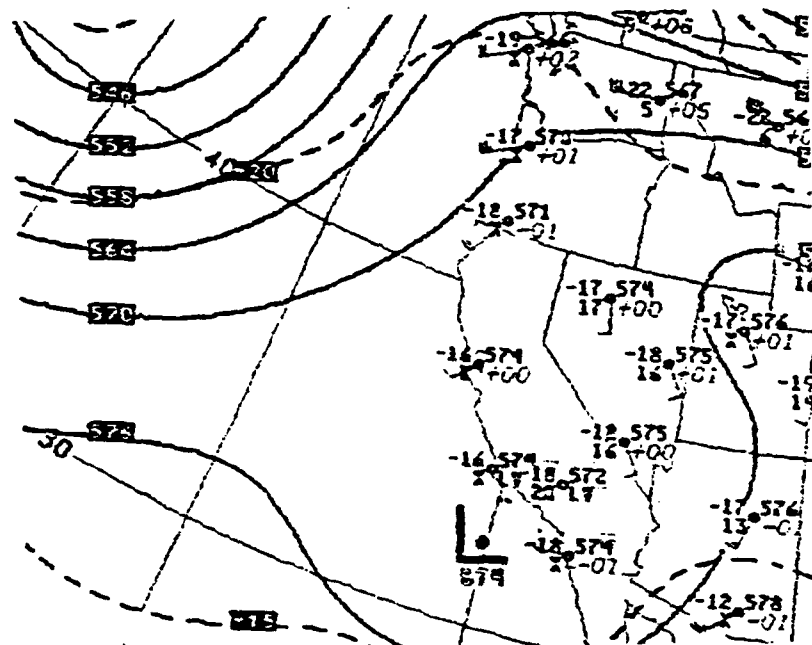


(b)

Figure 3.14 Surface (a) and 500 mb (b) analyses
1200 GMT 13 April 1977.

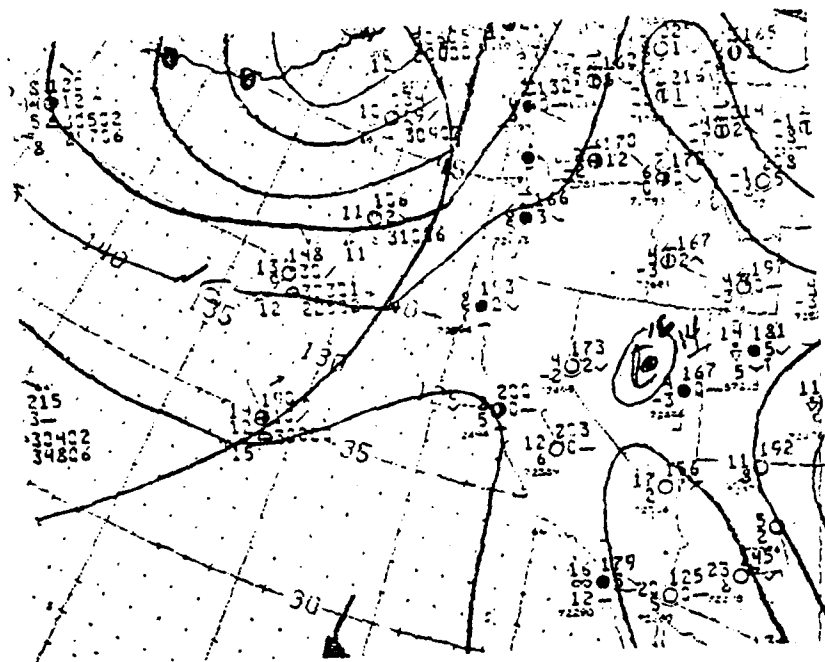


(a)

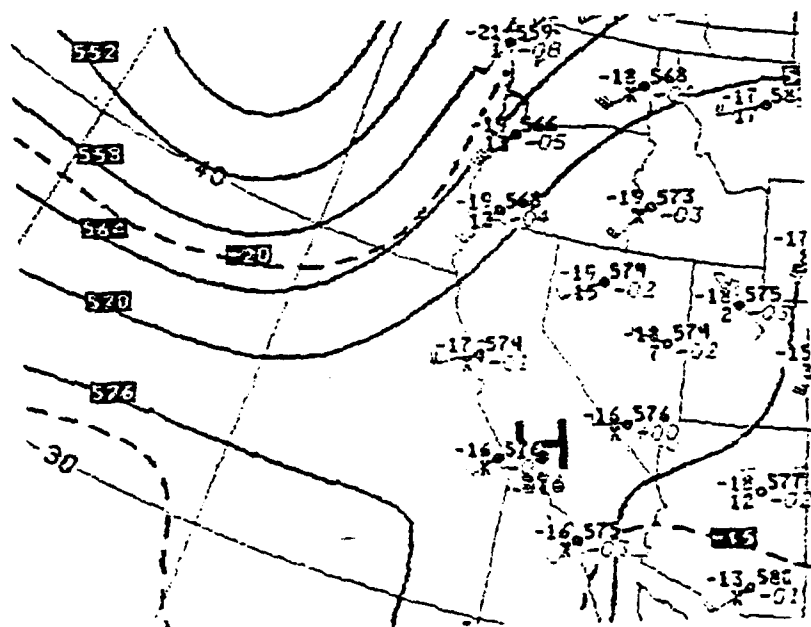


(b)

Figure 3.15 Surface (a) and 500 mb (b) analyses
1200 GMT 14 April 1977.

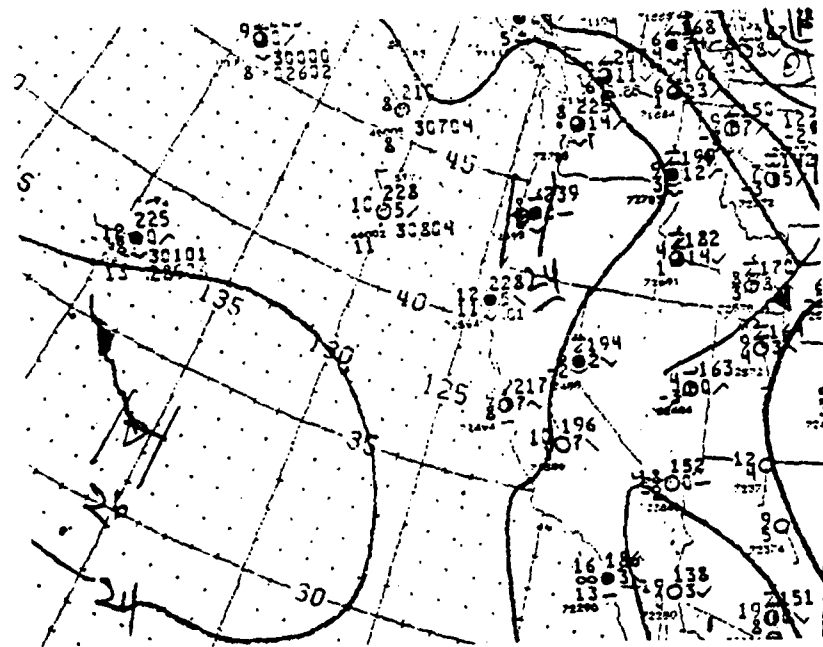


(a)

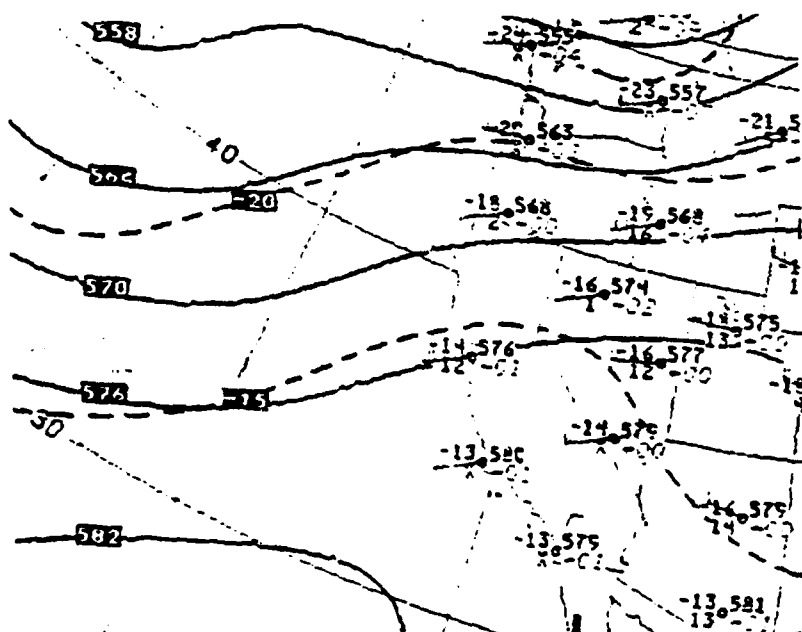


(b)

Figure 3.16 Surface (a) and 500 mb (b) analyses
1200 GMT 15 April 1977.



(a)



(b)

Figure 3.17 Surface (a) and 500 mb (b) analyses
1200 GMT 16 April 1977.

1745 13AP81 36A-2 00247 16032 WB2

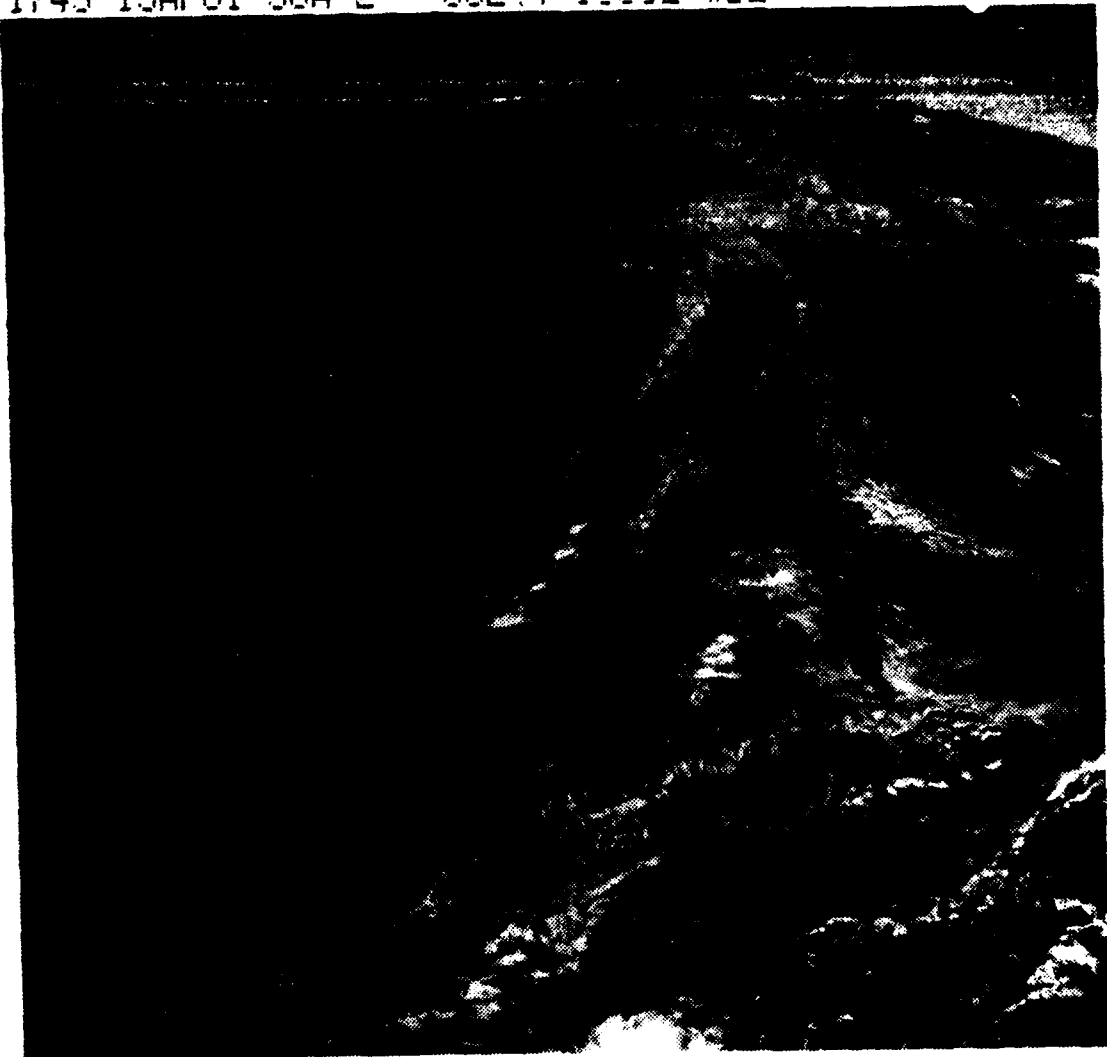


Figure 3.18 Satellite picture for 13 April 1981.

1745 14AP81 36A-2 00243 16021 WB2

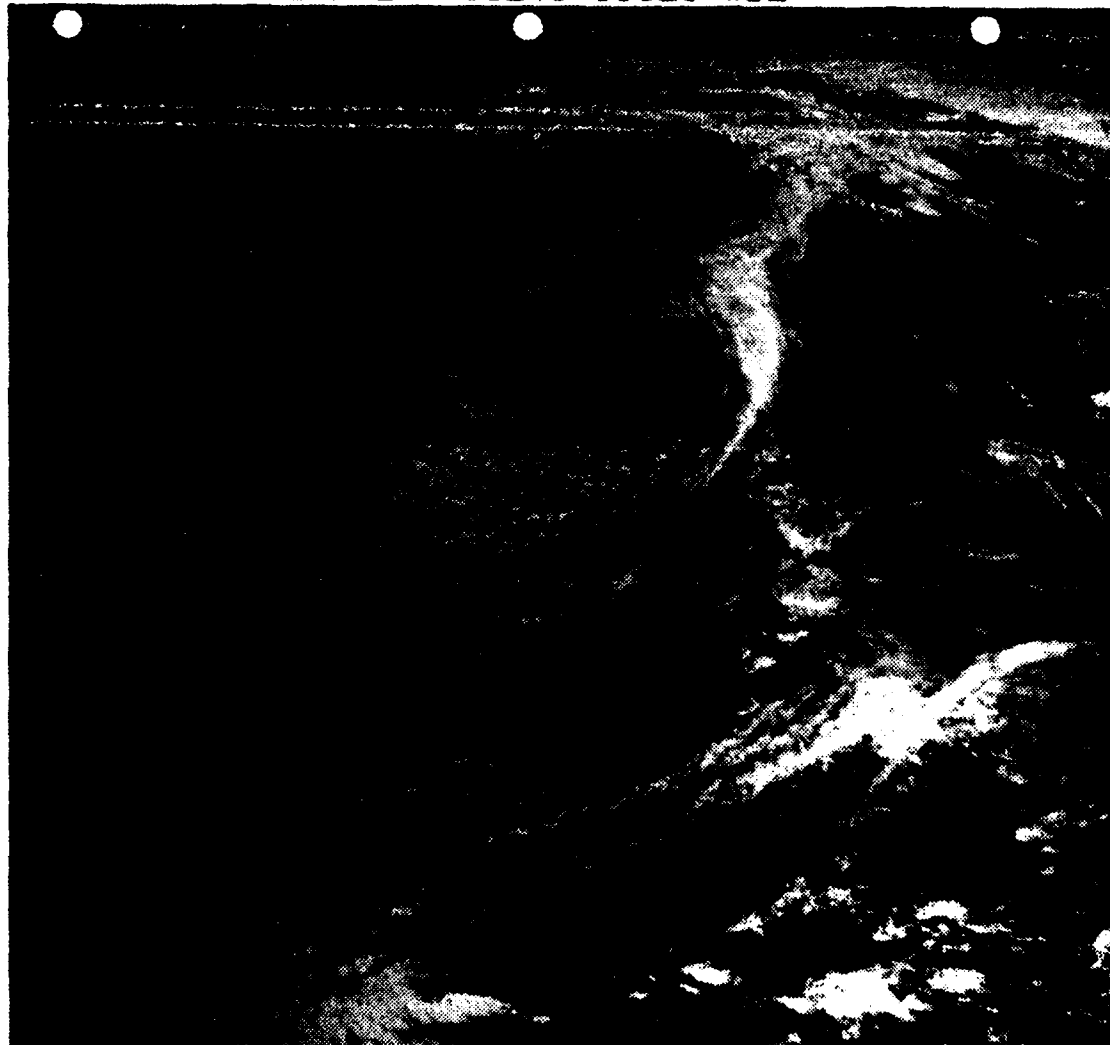


Figure 3.19 Satellite picture for 14 April 1981.

1745 15AP81 36A-2 00243 16002 WB2

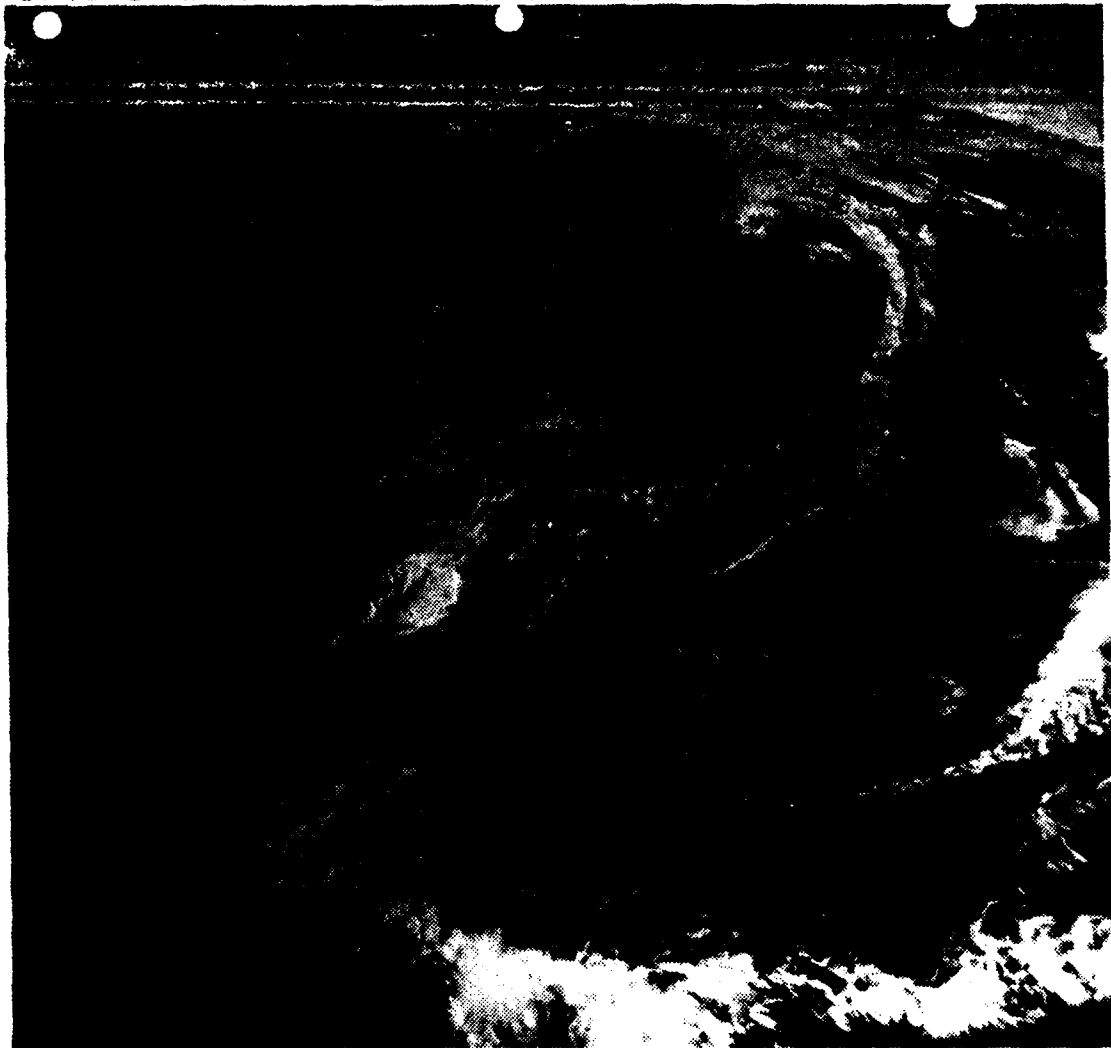


Figure 3.20 Satellite picture for 15 April 1981.

1745 16AP81 36A-2 00251 15982 WB2

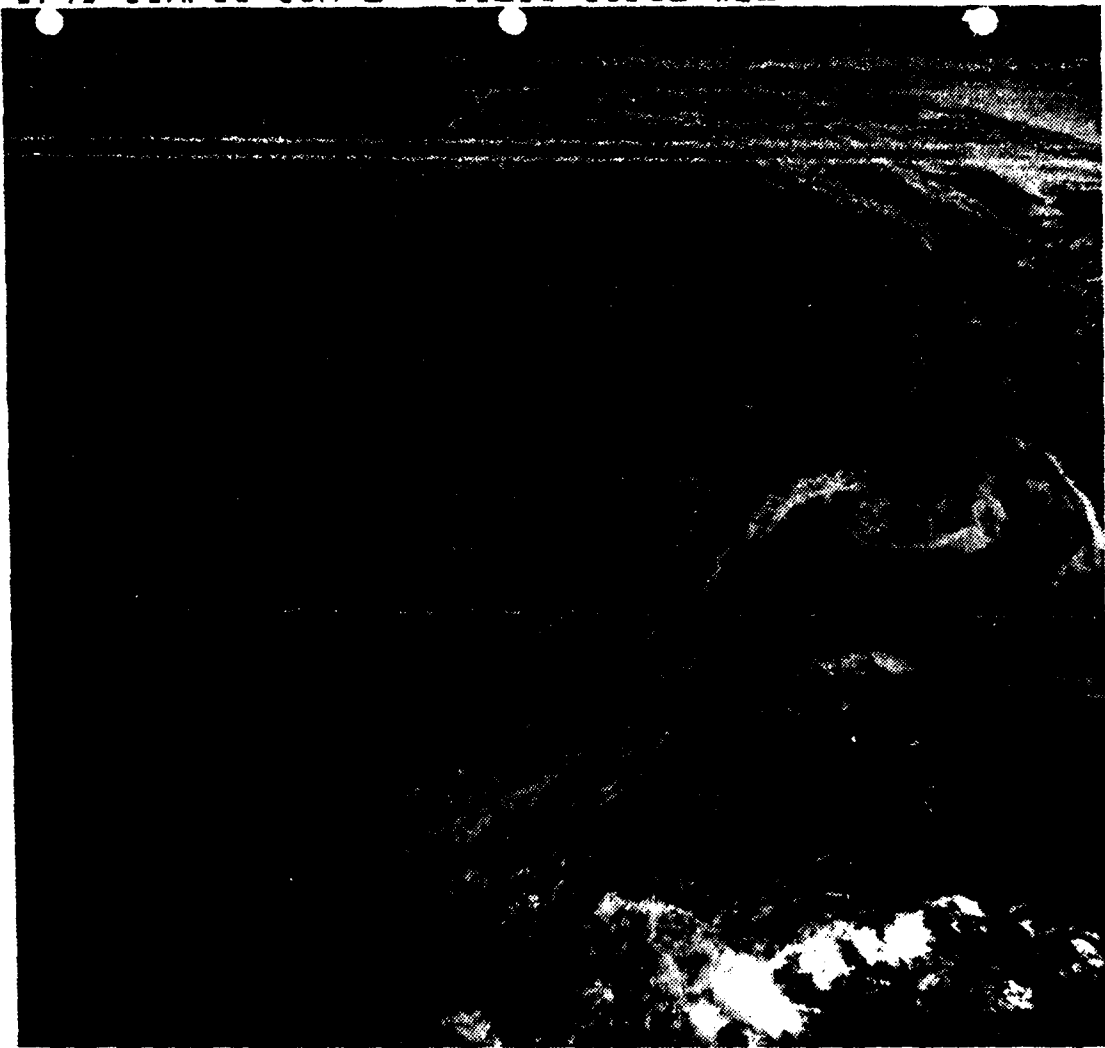


Figure 3.21 Satellite picture for 16 April 1981.

D. FALL CASE, PERIOD IV (29 AUGUST - 5 SEPTEMBER 1981)

The surface (a) and 500 mb (b) analyses for Period IV appear in Figs. 3.23 through 3.30. The predominate surface feature during this entire period was the presence of a high pressure system in the Eastern portions of the North Pacific Ocean. A thermal low and trough system dominated the southern California region. The effect of these two surface features was to produce weak onshore flow in the area of concern. Conclusions drawn from the 500 mb analyses show that, except for the last day of the period, the maximum westerly flow remained north of California. Only on 5 September did the Polar jet extend toward the regions of interest.

The surface analysis for 29 August (Fig 3.23) shows the western Pacific Ocean dominated by a high pressure system with a low pressure center located off the Washington coast. A thermal low extended northwestward from Mexico into California with troughing extending into northern California. The southern end of a cold front had also moved into the northern California area.

By 30 August the cold front had moved into southern California and the thermal low had changed its orientation. The Pacific high pressure system showed weak intensification with movement toward the northeast and had pushed inland by the 31st. The 31st also showed that the cold front was beginning to leave California but with another frontal system moving out of the Gulf of Alaska. Figures 3.24 through 3.25 depict these occurrences.

The 1 September analysis revealed a weakening of the high pressure and a cold front approaching California. A thermal trough was well established over California but very diffuse on 2 September as the cold front moved through

southern California. The high pressure system again intensified and showed no marked weakening throughout the remainder of the period. The only significant event after 2 September was the entrance of a rapidly moving cold front into California. This scenario is shown in Figs 3.26 through 3.30.

A sample of the rawinsondes for this period appears in Fig. 3.22. The rawinsondes for this period have a very good subsidence type inversion throughout the period. In each rawinsonde release the inversion was found above 1000 feet with decreasing relative humidity through the inversion zone.

The extent and development of the low clouds appear in the pictures in Figs. 3.31 and 3.38. The satellite pictures revealed a buildup of coastal low clouds (stratus and/or fog) during the period. Beginning on 29 August the clouds tended to be thin with some dissipation during the day. Further into the period the stratus thickens and by the end of the period there is a dense area of low clouds off the central and southern California coastal regions.

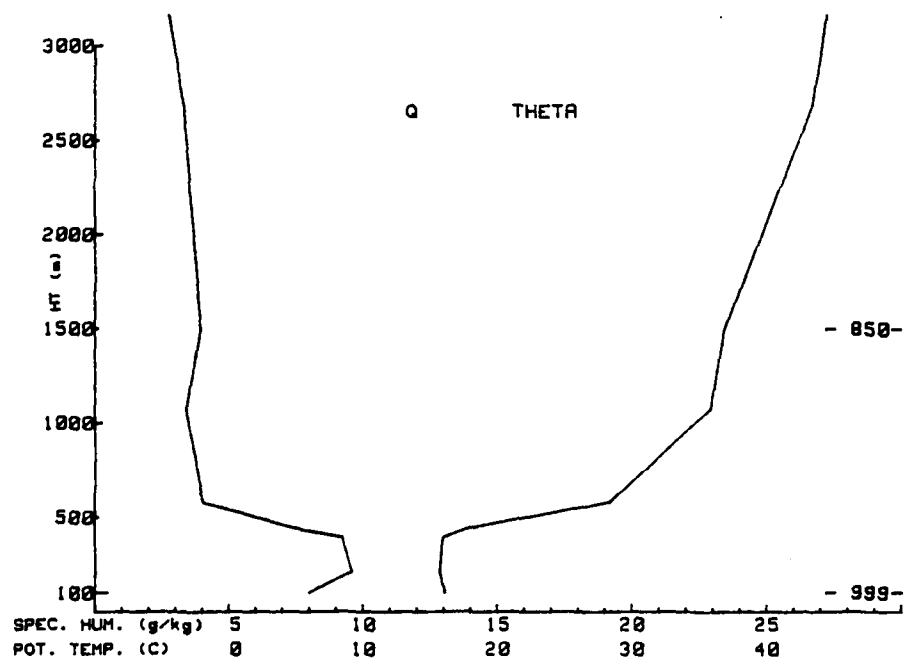
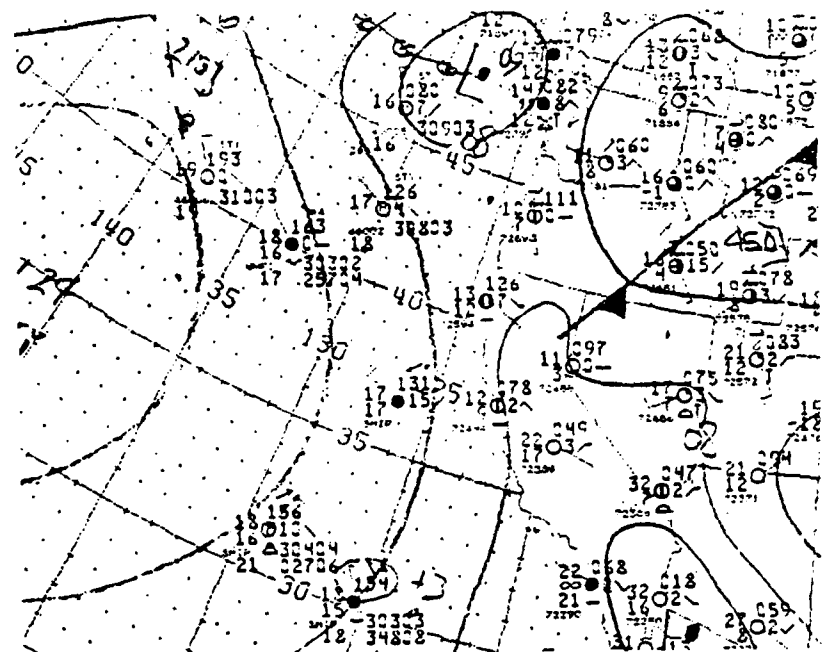
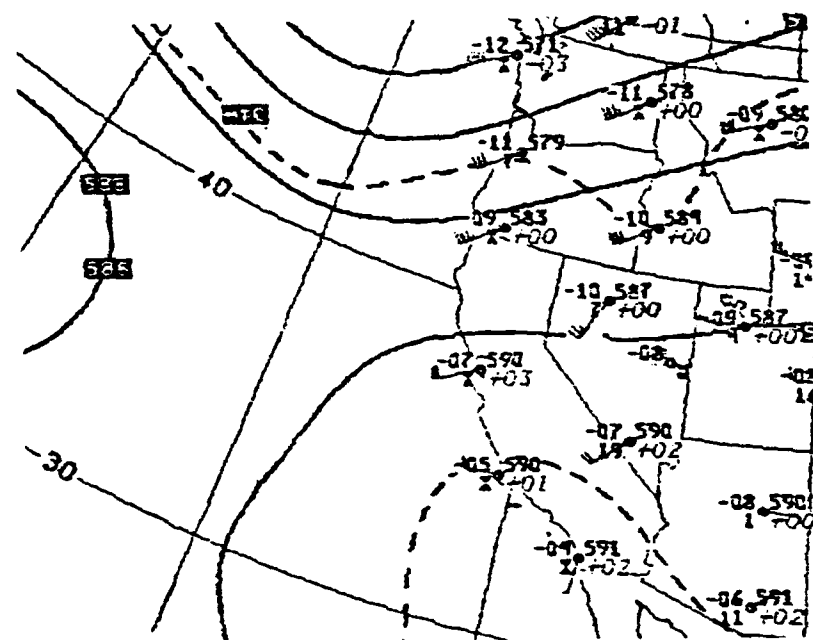


Figure 3.22 Rawinsonde example for Fall Case.

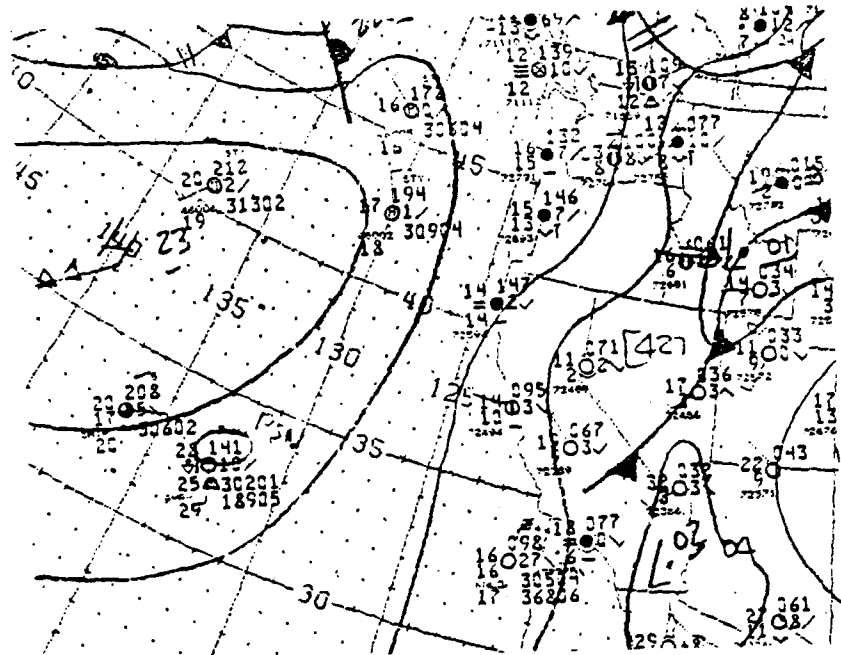


(a)

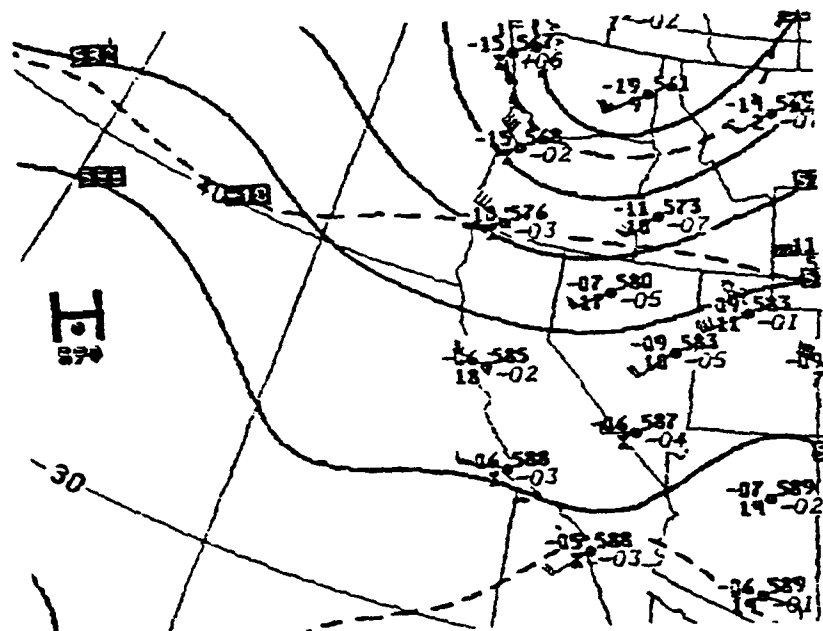


(b)

Figure 3.23 Surface (a) and 500 mb (b) analyses
1200 GMT 29 August 1977.

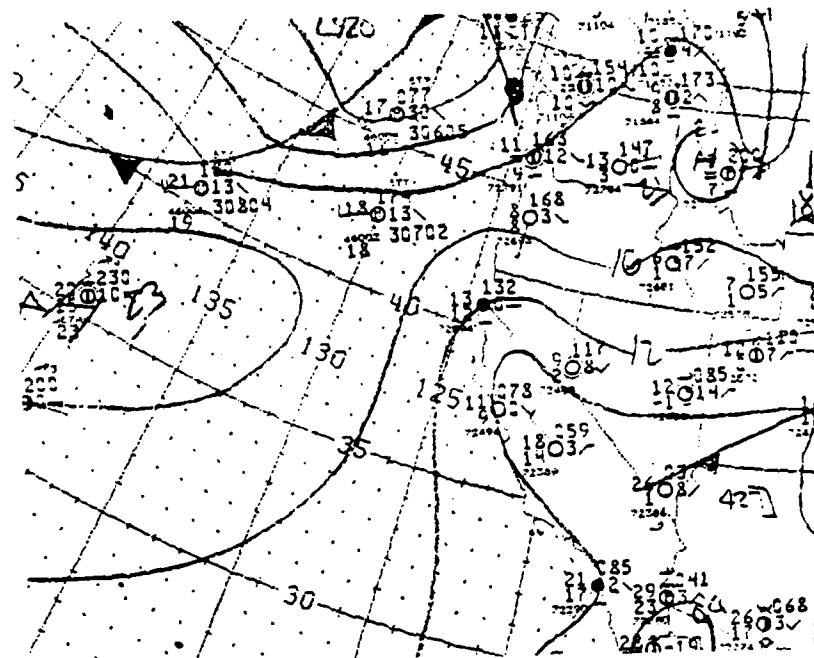


(a)

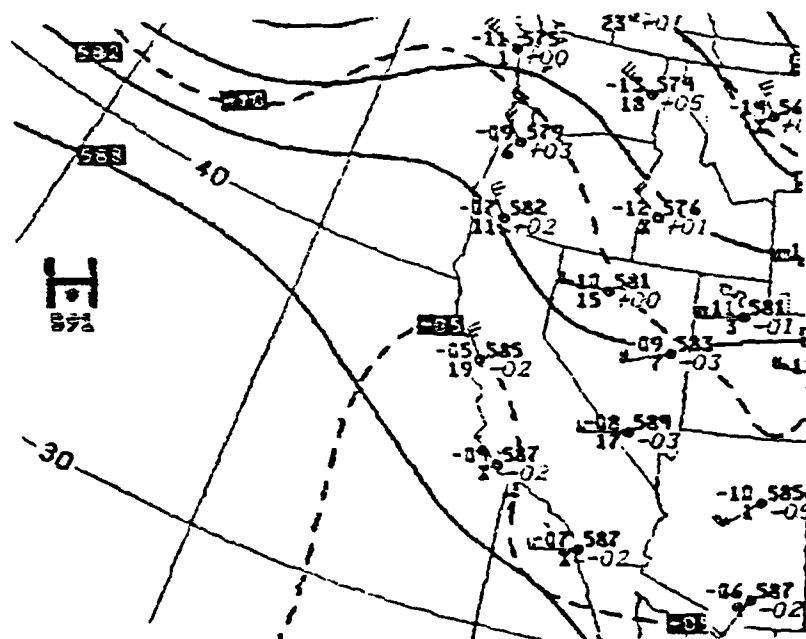


(b)

Figure 3.24 Surface (a) and 500 mb (b) analyses
1200 GMT 30 August 1977.

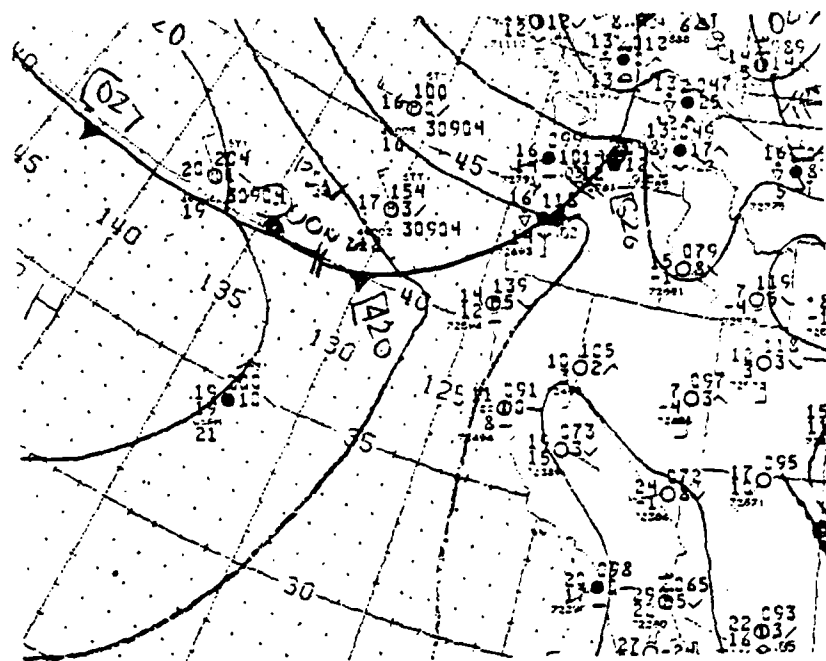


(a)

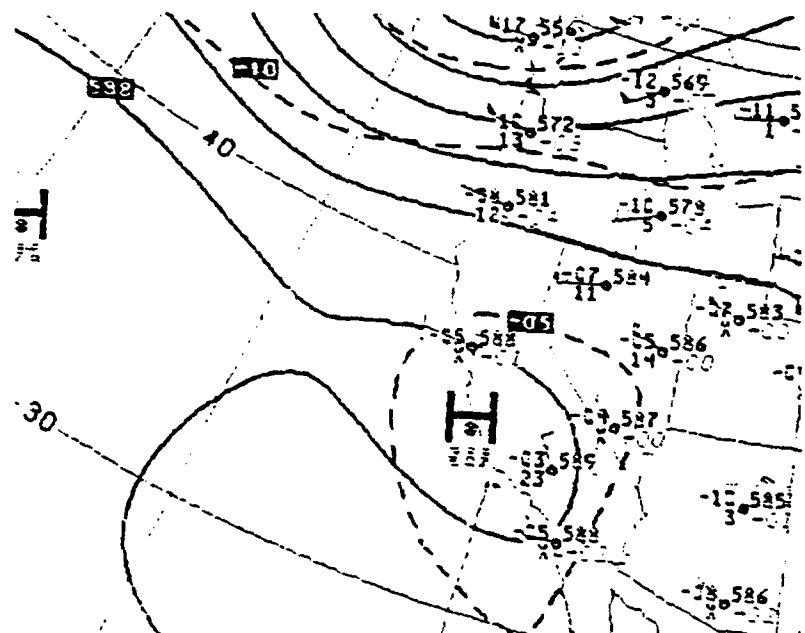


(b)

Figure 3.25 Surface (a) and 500 mb (b) analyses
1200 GMT 31 August 1977.

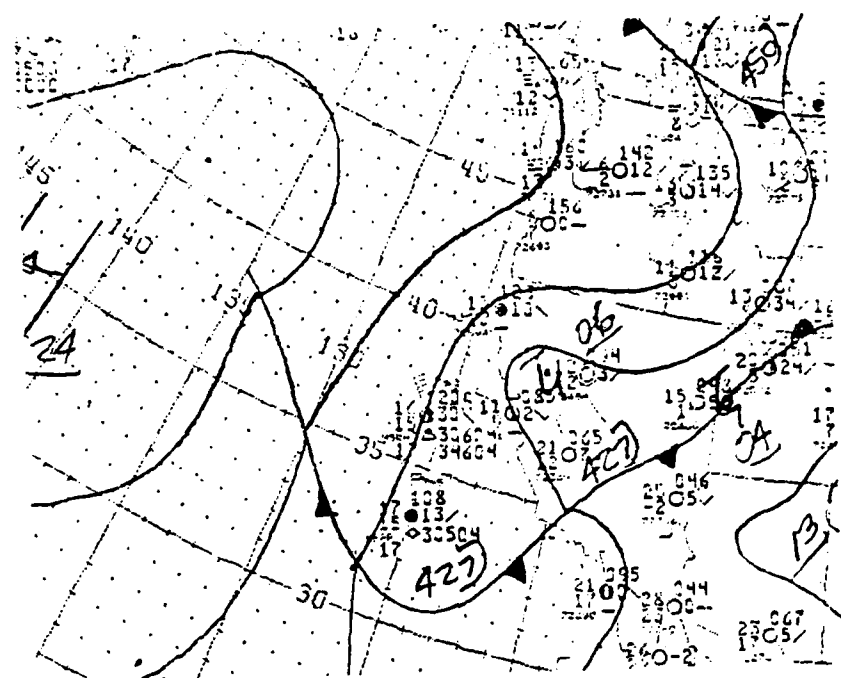


(a)

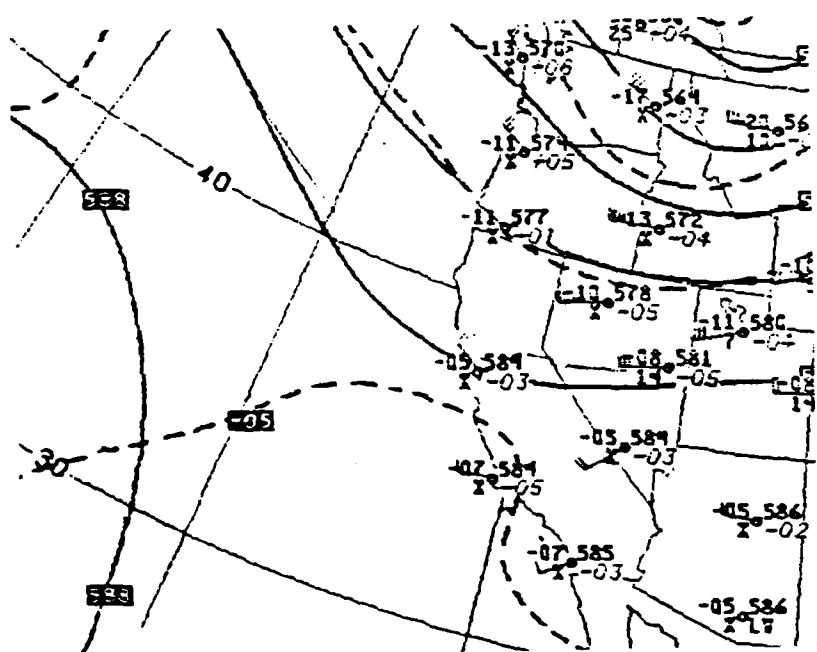


(b)

Figure 3.26 Surface (a) and 500 mb (b) analyses
1200 GMT 1 September 1977.

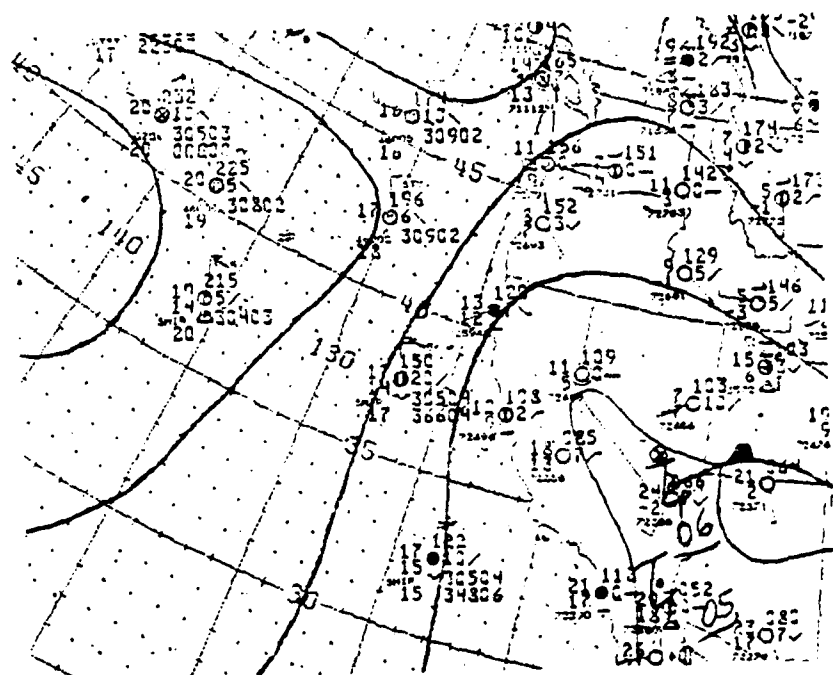


(a)

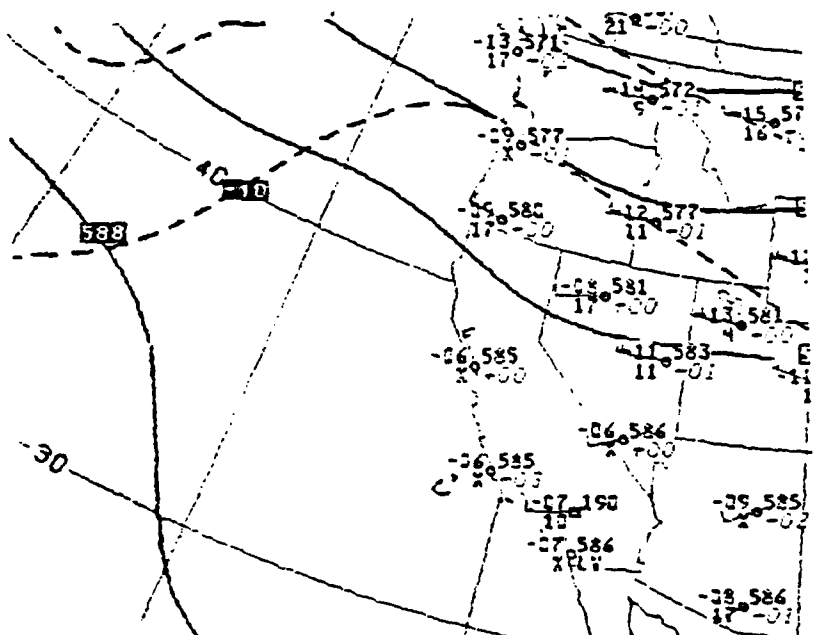


(b)

Figure 3.27 Surface (a) and 500 mb (b) analyses
1200 GMT 2 September 1977.

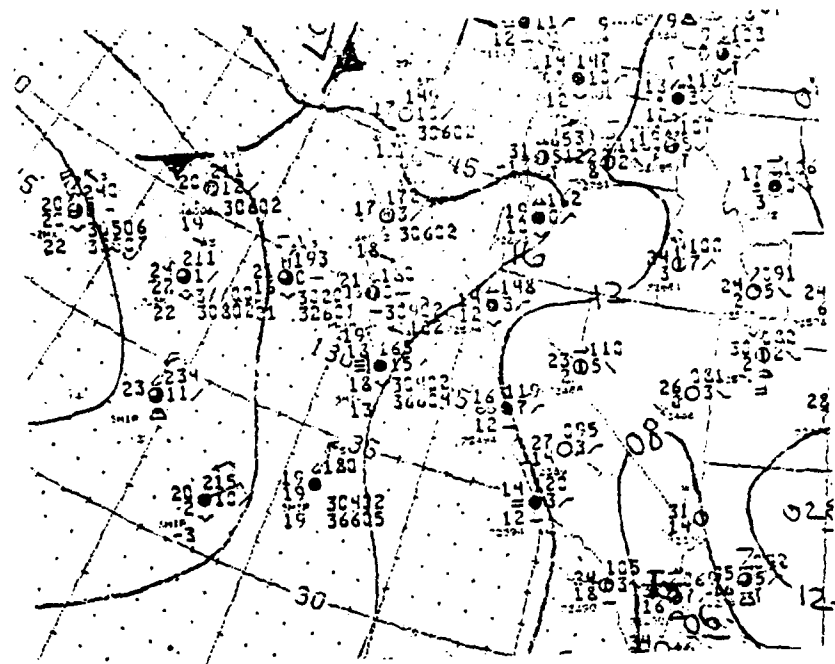


(a)

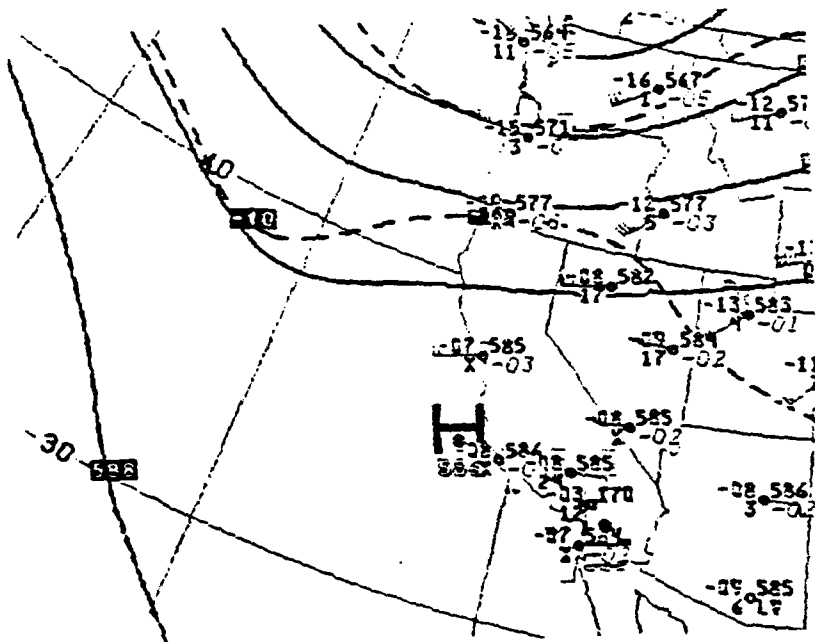


(b)

Figure 3.28 Surface (a) and 500 mb (b) analyses
1200 GMT 3 September 1977.

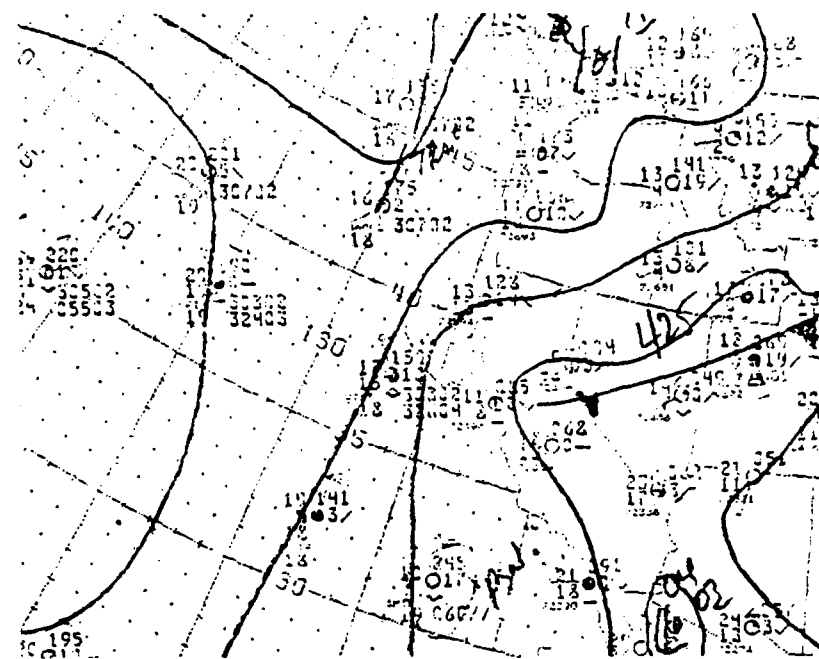


(a)

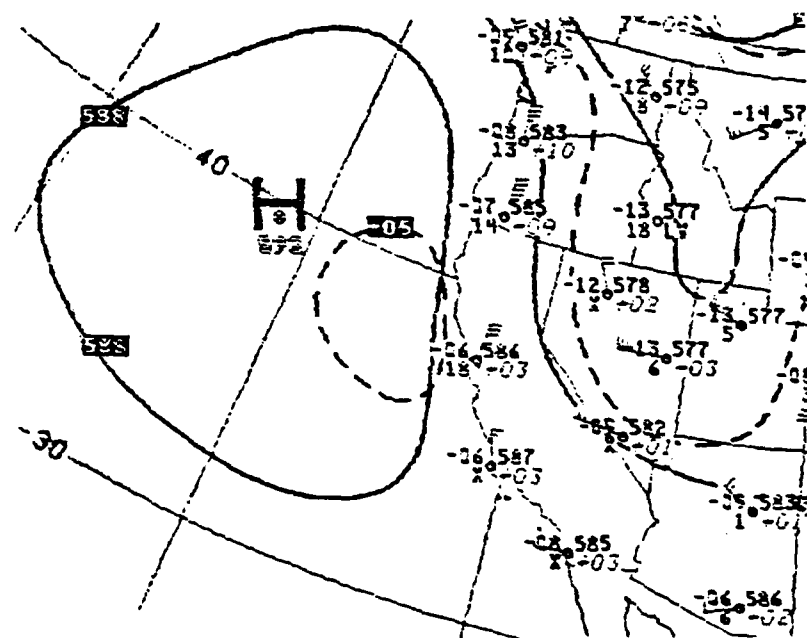


(b)

Figure 3.29 Surface (a) and 500 mb (b) analyses
1200 GMT 4 September 1977.



(a)



(b)

Figure 3.30 Surface (a) and 500 mb (b) analyses
1200 GMT 5 September 1977.

1500 29AU81 17A-2 C1163 14831 WB1

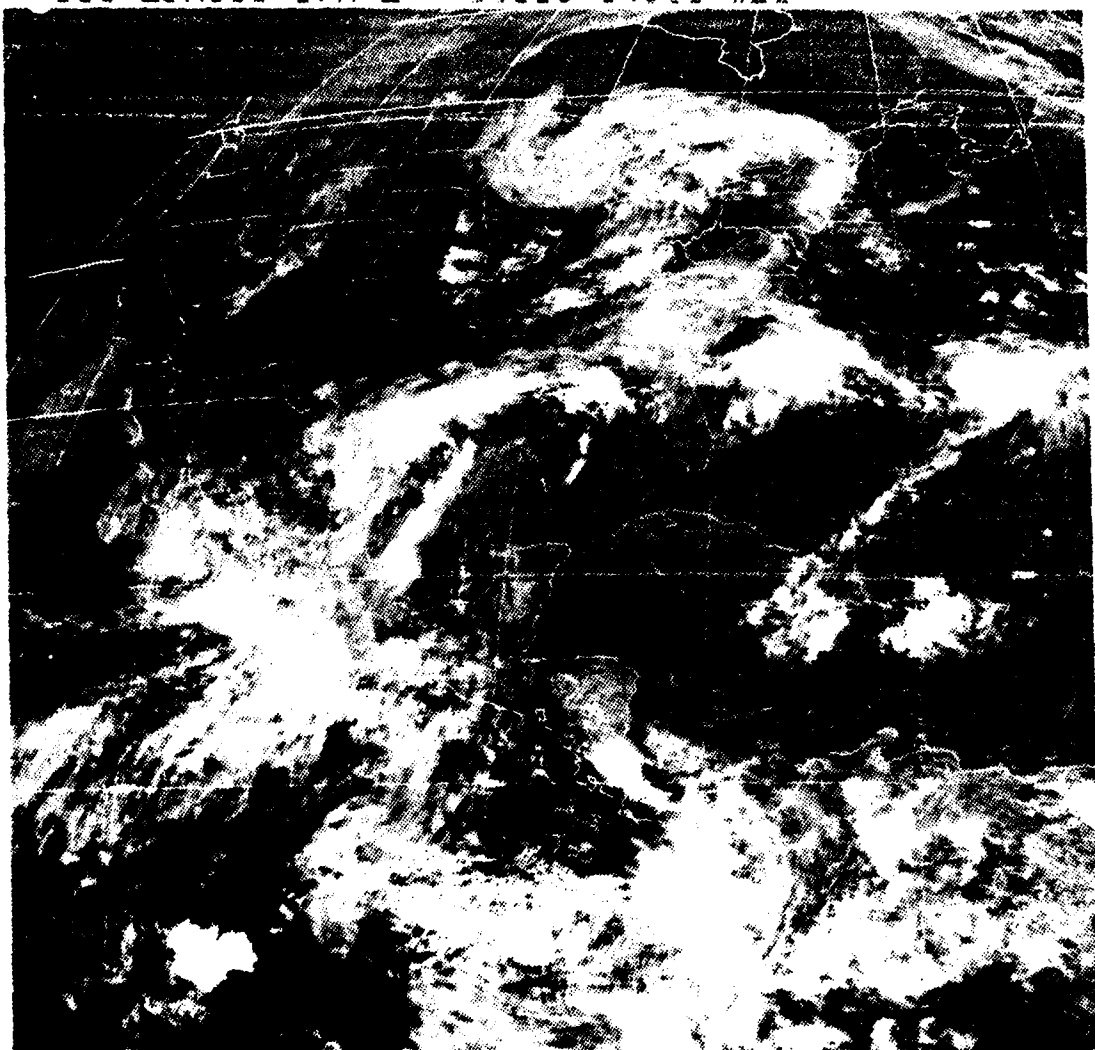


Figure 3.31 Satellite picture for 29 August 1981.

1745 30AU81 36A-2 00221 15991 WB2

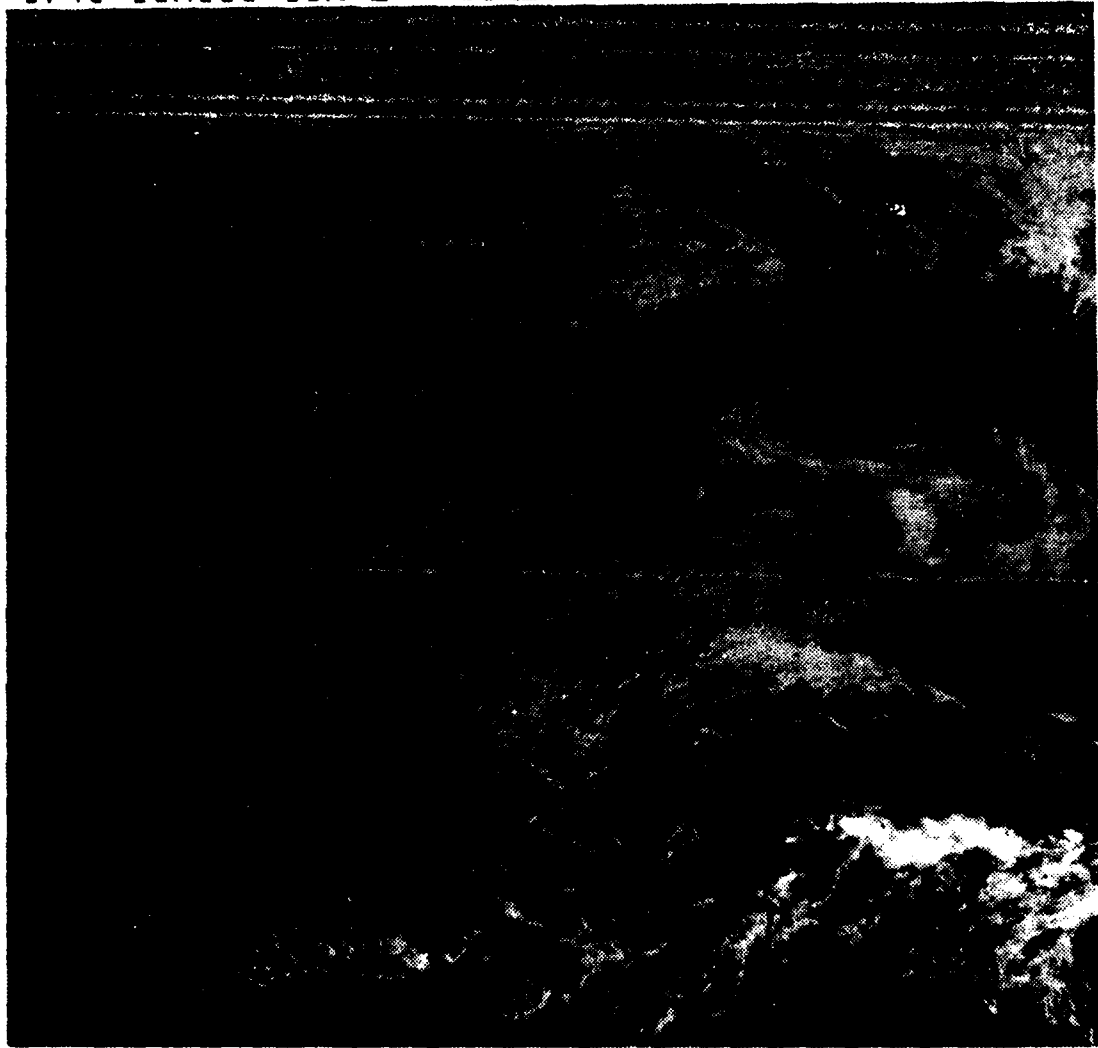


Figure 3.32 Satellite picture for 30 August 1981.

1745 31AU81 36A-2 00213 15992 WB2



Figure 3.33 Satellite picture for 31 August.

1745 01SE81 36A-4 00332 19161 UC2

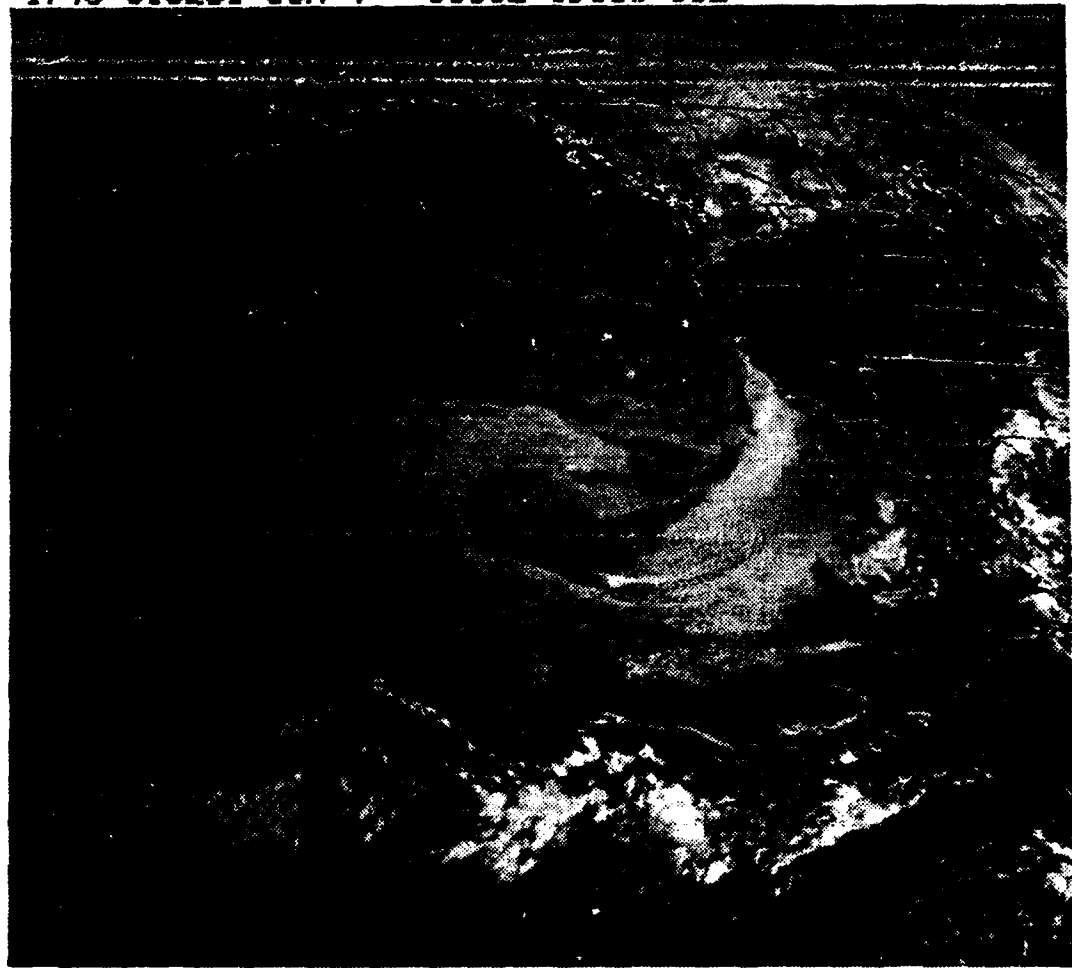


Figure 3.34 Satellite picture for 1 September 1981.

1745 02SE81 36A-2 002.4 16002 WB2

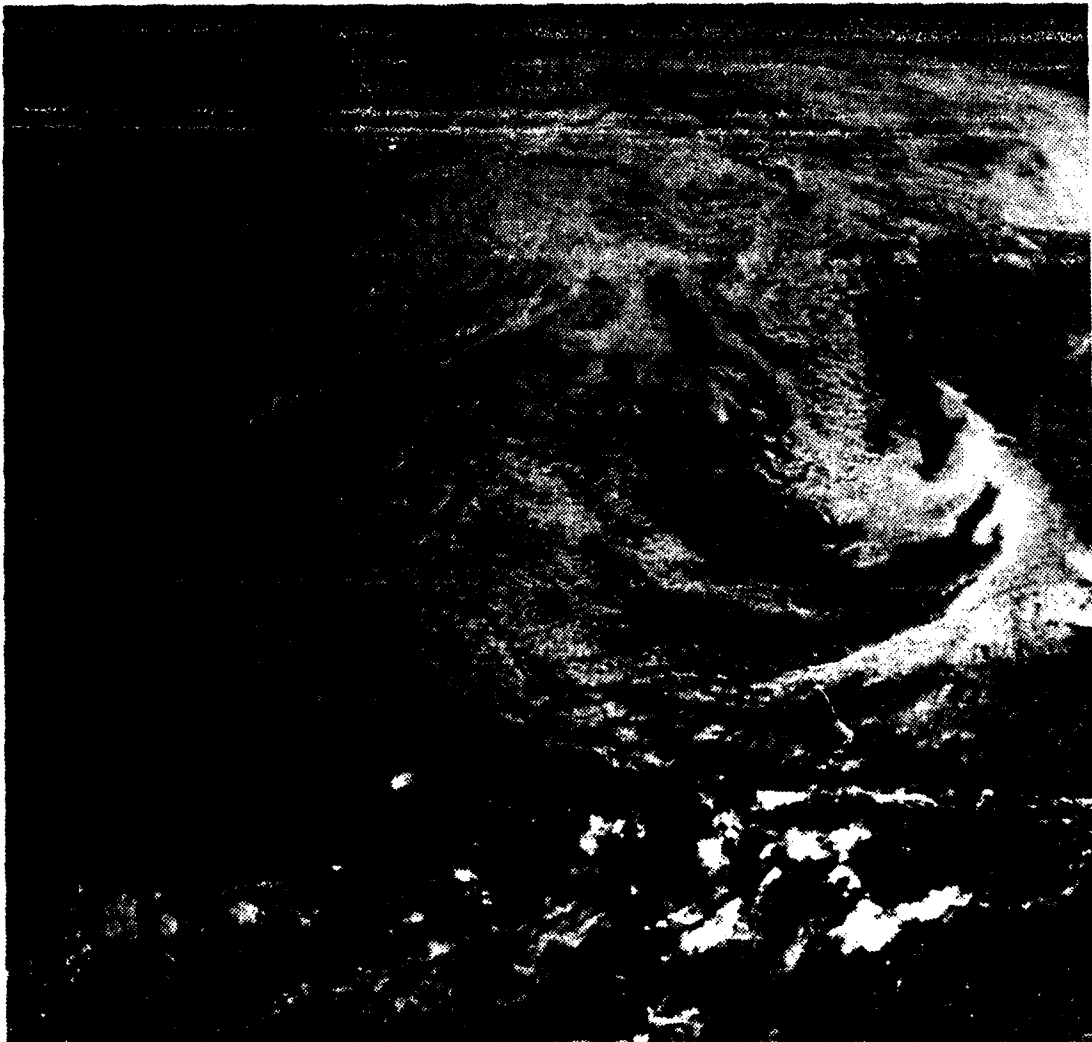


Figure 3.35 Satellite picture for 2 September 1981.

1715 03SE81 36A-2 00222 16011 WB2

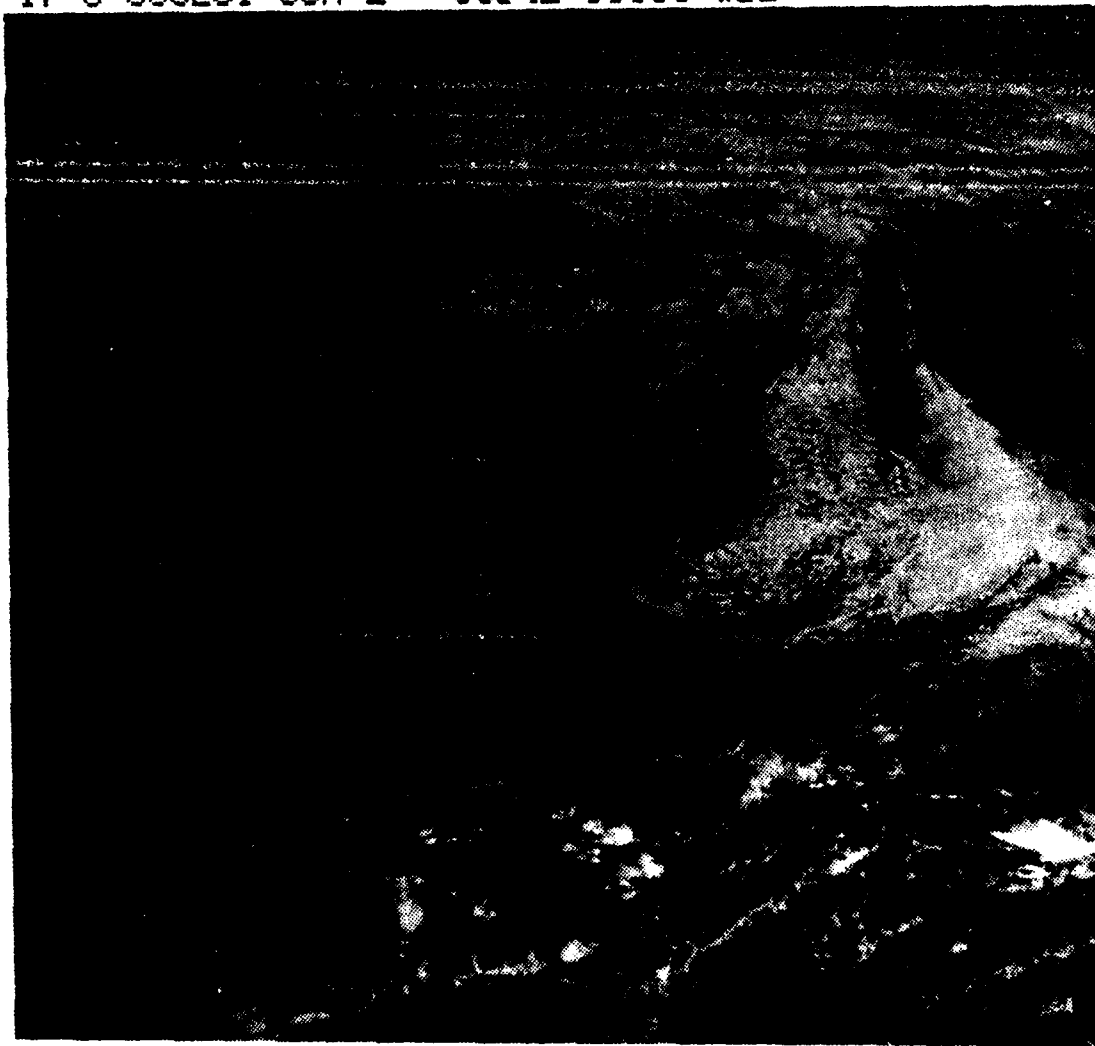


Figure 3.36 Satellite picture for 3 September 1981.

1745 04SE81 36A-2 00222 16021 WB2

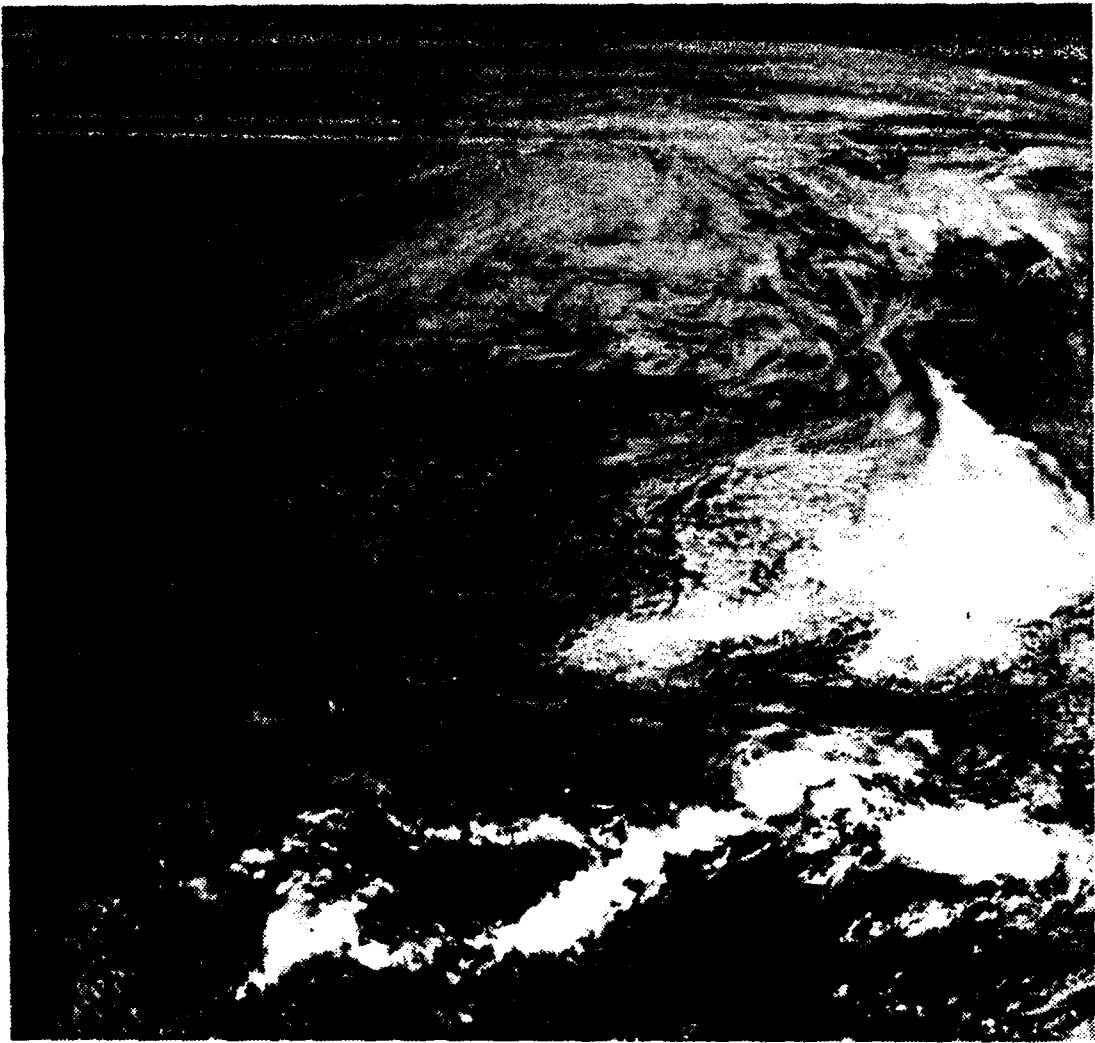


Figure 3.37 Satellite picture for 4 September 1981.

1:45 05SE81 36A-2 0022 16022 WB2

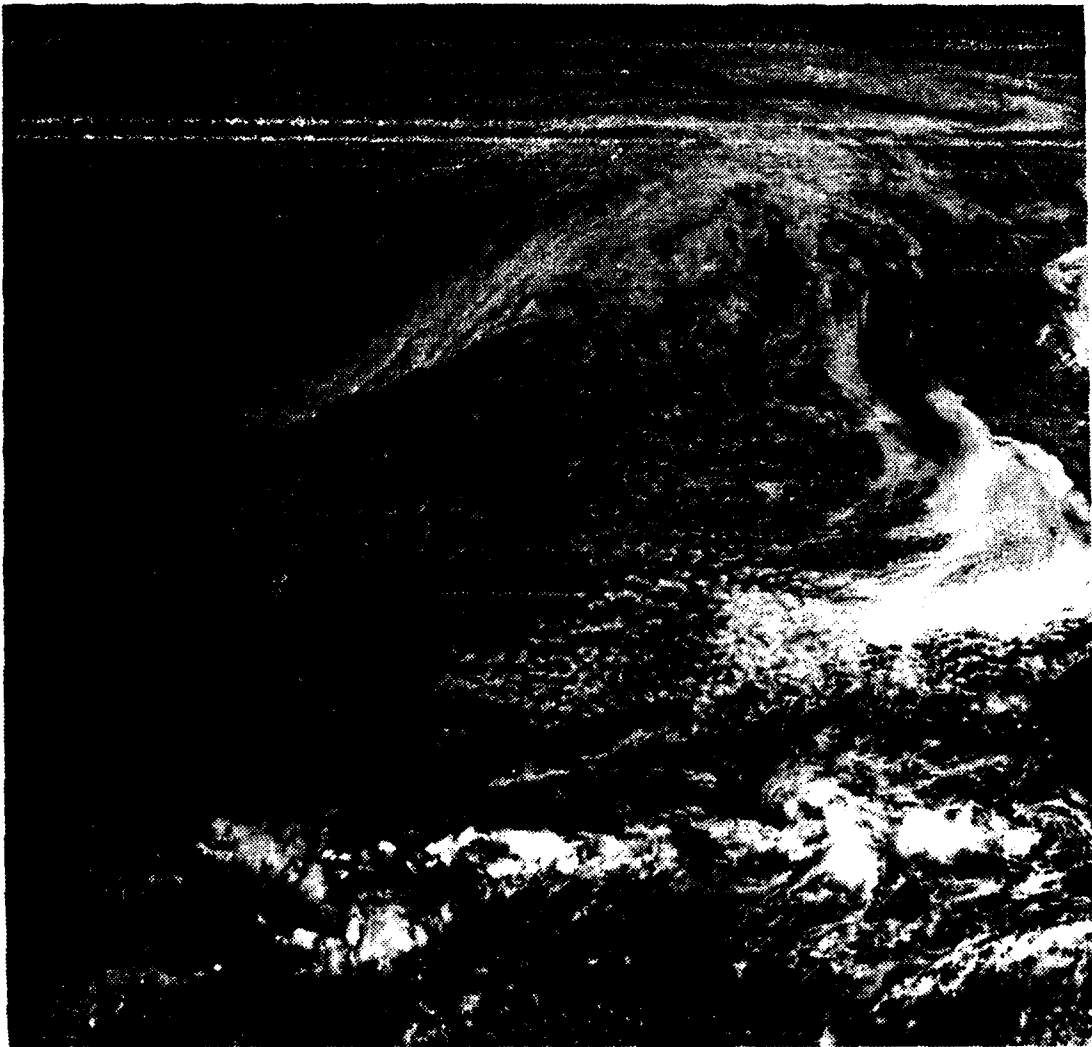


Figure 3.38 Satellite picture for 5 September 1981.

IV. RESULTS

Model forecasts were made for every 30 minutes for 24 hours following the initialization time. The forecasts presented in the following tables show only the 12 and 24 hour values since they correspond to the verification times. The structure of the tables are such that the first forecast, indicated by column heading FCST1, was based on the first observation for initialization and within that column are the forecasts generated. For example, if the first observation was for 1/0000 GMT then the forecasts from that observation would be for 1/1200 GMT and 2/0000 GMT. These forecasts would be in column FCST1. The second forecast, column heading FCST2, was initialized with the second observation (e.g., 1/1200 GMT) and within that column are the forecasts generated (2/0000 GMT and 2/1200 GMT). Each table continues in this manner until all forecasts for a period have been given.

Root mean square (RMS) scores are given following each forecast except the last. No RMS for the last forecast were given as there were no observations for comparison. Also note that the 12 hour RMS value simply represents the difference between observed and forecasted values.

The values given in the tables are for the parameters: inversion height, lifting condensation level, mixed layer potential temperature and mixed layer specific humidity. Units for these are meters for the inversion height and the lifting condensation level, degrees Centigrade for potential temperature, and g/kg for specific humidity. Also note that subsidence, used in discussing these results, are given in Table I.

A. DISCUSSION OF MODEL RESULTS FOR PERIOD I (SUMMER)

This period was dominated by clear skies. The forecast lifting condensation level values (see Table III) only forecasted clouds during FCST2. The forecasted inversion heights, Table II, reveal that the model was either very close or quite in error relative to the observed height. Tables IV and V reveal that, throughout the period, there were also problems associated with potential temperature and

TABLE II
July Inversion Results

DATE	GMT	CBS	FCST1	RMS	FCST2	RMS	FCST3	RMS
25	00	356	-	-	-	-	-	-
	12	157	195	38.0	-	-	-	-
26	00	277	108	173.2	92	185.0	-	-
	12	199	-	-	112	204.4	165	34.0
27	00	206	-	-	-	-	100	111.3
DATE	GMT	CBS	FCST4	RMS	FCST5	RMS	FCST6	RMS
27	00	206	172	34.0	-	-	-	-
	12	120	146	42.8	154	34.0	-	-
28	00	199	-	-	116	89.7	71	128.0
	12	-	-	-	-	-	42	-
29	00	-	-	-	-	-	-	110
								62

TABLE III
July Lifting Condensation Levels

DATE	GMT	OBS	FCST1	FCST2	FCST3	FCST4
25	00	633	-	-	-	-
	12	146	299	-	-	-
26	00	1119	199	42	-	-
	12	217	-	0	519	-
27	00	206	-	-	309	185
	12	452	-	-	-	168
DATE	GMT	OBS	FCST5	FCST6	FCST7	
27	12	452	605	-	-	
28	00	1261	410	184	-	
	12	-	-	176	586	
29	00	-	-	-	366	

TABLE IV
July Potential Temperatures

DATE	GMT	OBS	FCST1	FCST2	FCST 3	FCST4
25	00	16.2	-	-	-	-
	12	11.6	17.4	-	-	-
26	00	17.4	18.2	11.6	-	-
	12	12.6	-	8.5	17.8	-
27	00	20.9	-	-	18.4	15.2
	12	14.1	-	-	-	16.7
DATE	GMT	OBS	FCST5	FCST6	FCST7	
27	12	14.1	19.8	-	-	
	00	19.5	19.6	17.1	-	
28	12	-	-	18.3	18.9	
	00	-	-	-	19.3	

TABLE V
July Moisture Values

DATE	GMT	OBS	FCST1	FCST2	FCST3	FCST4
25	00	8.2	-	-	-	-
	12	7.9	6.3	-	-	-
26	00	6.8	5.4	8.3	-	-
	12	8.1	-	7.2	9.7	-
27	00	9.3	-	-	11.3	9.8
	12	7.9	-	-	-	10.8
DATE	GMT	OBS	FCST5	FCST6	FCST7	
27	12	7.9	10.6	-	-	
	00	7.3	11.6	11.1	-	
28	12	-	-	12.0	10.1	
	00	-	-	-	11.6	

specific humidity forecasts. These problems will be covered during the following discussions.

Examination of the inversion height results reveals some good and some poor height forecasts at the 12 hour point but mostly bad forecasts at 24 hours. Those forecasts made with average subsidence rates (-0.003 to -0.005 m/s) had fair to good results at 12 hours but had poor results at 24 hours. The best height forecasts (Table II column FCST4) were with the weakest subsidence rate while the second best (the fifth forecast) was with the strongest subsidence rate. Also of interest is that forecasts with the strongest subsidence

also had the lifting condensation level well above the inversion. Another important feature in Table II is that, except for the forecast with the weakest subsidence, the best forecasts were for the 12 hour periods initialized at 1200 GMT (a morning period for the California region).

Potential temperature, specific humidity, radiation (with and without clouds) and entrainment will be examined in explaining what was occurring with the predicted inversion heights for this period. Each parameter will be described separately as to its possible impact on the inversion forecast.

1) potential temperature - Under clear skies one would normally expect nightly cooling over land. The observed values shown in Table IV reveal that this occurred yet the forecasts do not reflect this fact. Nocturnal cooling strengthens the jump and when coupled with subsidence lowers the inversion as seen in Fig. 4.1. All forecasts were lowering the inversion due to good subsidence rates for initialization. Daytime heating acts against the subsidence, weakens the jump, and results in lifting of the inversion. This diurnal event was not reflected in the forecasts.

2) specific humidity - After the first two forecasts, specific humidity forecast values were only fair. There were no forecast values which were good since the errors ranged from just under 1 g/kg up to 3.3 g/kg. The primary trend in the forecasts was to increase specific humidity. This prediction of too large a specific humidity caused the model to predict even lower lifting condensation levels which, in turn, enhances the poor inversion predictions.

3) radiation - This factor must be considered under conditions of clear as well as cloudy skies.

a) cloudy - In the second forecast the model predicted clouds to form and extend to the surface. The clouds radiate long wave energy to space so the potential temperatures were forecast too low. Inversion predictions, while decreasing then increasing during this forecast, did not reflect the diurnal change predominate with clear skies.

b) clear - Radiation computations here could have been incorrectly influenced by the large specific humidity forecasts. This accompanied with good subsidence rates caused all forecasts to lower the inversion.

4) entrainment rates - these influence the time rate of change of specific humidity and potential temperature as well as inversion height. In several of the forecasts the entrainment rate was zero so it was internally set to a positive, yet minimal, value. This could have affected the other forecasted values but it is believed the effect was less than others.

A definite diurnal pattern can be seen (see Fig. 4.1) in the observed inversion heights. Generally there were increased heights in the transition from morning to evening and decreases for the opposite transition. This pattern coincides with the diurnal pattern of the potential temperatures which reflect radiative daytime heating and nightly cooling. Surface winds also displayed the influence of daily heating with evening reports having the strongest wind speeds and with steady northwesterly directions (an onshore wind). Figure 4.1 also depicts the 12 and 24 hour forecasts and it is easily seen that the diurnal pattern shown by the

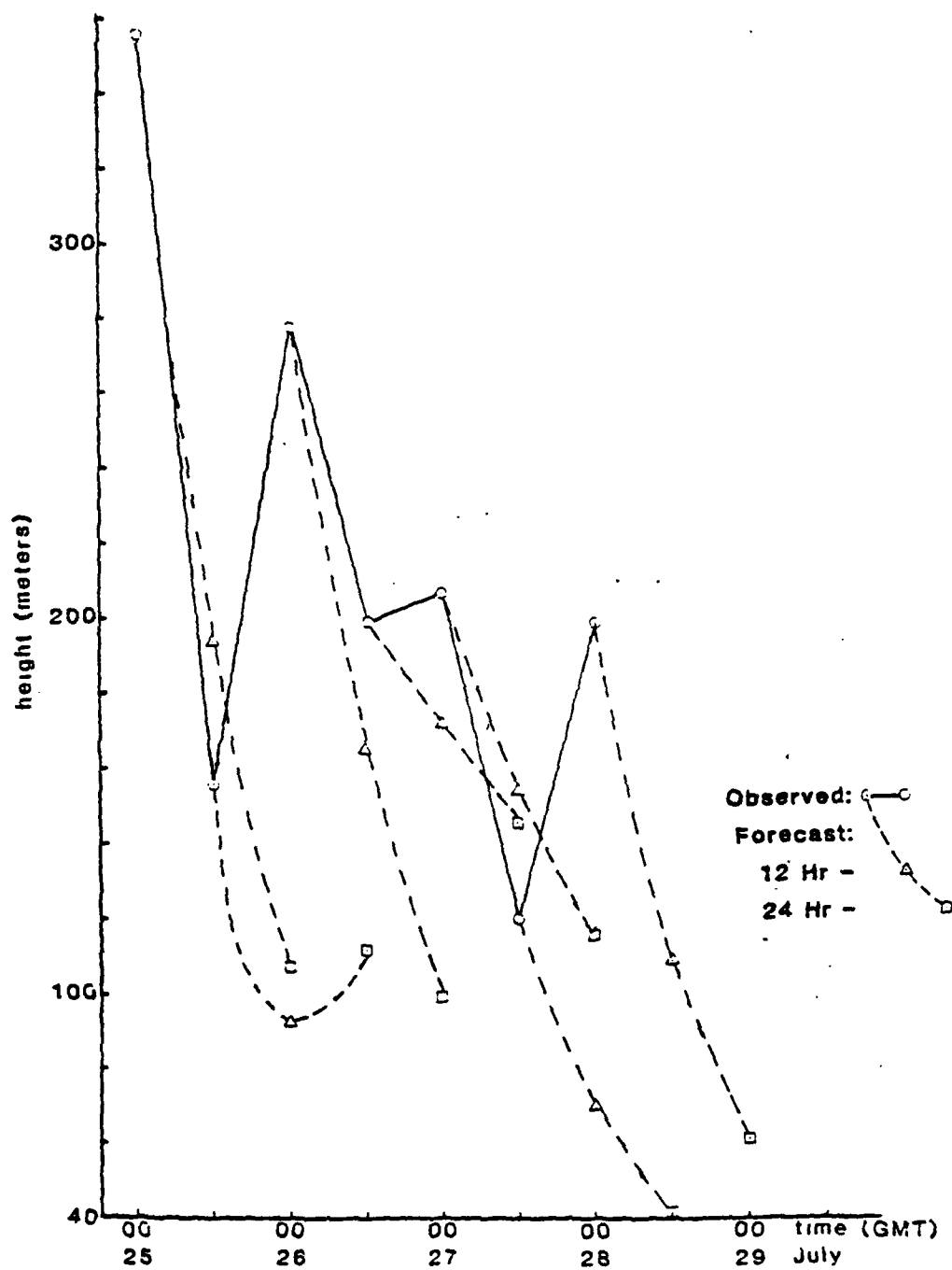


Figure 4.1 Graphical Depiction of Summer Case Observed and Forecasted Inversion Heights.

observed data is not shown by the forecasts. Only the morning to evening 12 hour forecast indicate a correct trend. However close inspection of the forecasts indicate that at these times the model inputs for subsidence were strong thereby influencing the forecast.

These effects all suggest problems with the radiation calculations throughout this summer period. A reason for this error is the fact that Vandenberg AFB is a shoreline station and the model is primarily designed for over water use. Therefore, land heating and cooling by solar radiation, even through a stratus sky, require adjustments to apply the model at a shoreline station. Vertical velocity and entrainment rates also affected forecasted MABL properties through influences on the rate of change of key parameters as well as the inversion heights (see Eqn. 2.3).

B. DISCUSSION OF MODEL RESULTS FOR PERIOD II (WINTER)

Results in Table VI generally suggest that during this season the model fails to forecast variations in the height of the inversion. Tables VII through IX compare forecast and observed lifting condensation levels, potential temperatures and specific humidity values.

TABLE VI
December Inversion Results

DATE	GMT	CBS	FCST1	RMS	FCST2	RMS	FCST3	RMS	FCST4
13	00	164	-	-	-	-	-	-	-
	12	171	45	126.0	-	-	-	-	-
14	00	284	14	210.7	40	244.0	-	-	-
	12	297	-	-	11	265.8	187	110.0	-
15	00	-	-	-	-	-	124	-	492
	12	-	-	-	-	-	-	-	623

TABLE VII
December Lifting Condensation Levels

DATE	GMT	OBS	FCST1	FCST2	FCST3	FCST4
13	00	1083	-	-	-	-
	12	2055	123	-	-	-
14	00	1056	22	936	-	-
	12	174	-	338	511	-
15	00	-	-	-	255	0
	12	-	-	-	-	0

TABLE VIII
December Potential Temperatures

DATE	GMT	OBS	FCST1	FCST2	FCST3	FCST4
13	00	17.2	-	-	-	-
	12	15.8	14.6	-	-	-
14	00	15.7	14.1	15.4	-	-
	12	13.0	-	15.2	14.9	-
15	00	-	-	-	14.8	8.2
	12	-	-	-	-	5.4

TABLE IX
December Moisture Values

DATE	GMT	OBS	FCST1	FCST2	FCST3	FCST4
13	00	8.9	-	-	-	-
	12	3.6	9.7	-	-	-
14	00	6.3	9.9	6.6	-	-
	12	8.3	-	9.0	8.0	-
15	00	-	-	-	9.2	7.3
	12	-	-	-	-	7.0

Vandenberg AFB remained under clear skies in this period yet the forecasts were for rapid formation of clouds. Forecast specific humidity values improved in the second forecast but were still not acceptable for the entire period. The potential temperature forecasts were best at the 12 hour point.

The primary causes for the poor performance of the model in this case appear to be vertical velocity and entrainment. The radiation and cloud calculations contributed to the error, but to a lesser extent. Entrainment was a key factor during the first three forecasts because null values were obtained in computation, so minimal positive values were assigned. The radiation segment calculations are strongly influenced by the presence of clouds and on the last day the model forecast clouds. With zero vertical velocity, the model forecast rapid lifting of the inversion. With no observations it is hard to evaluate those forecasts but the trend was for increasing heights although not as rapidly as predicted.

Forecast and observed heights for this period appear in Figure 4.2. The diurnal variations noted in the summer case are not present in this case. It is believed that the large errors in the inversion height forecasts are due to two factors. First, the vertical velocities with which the runs were initialized were large which lead to forecasts of lowering heights in all but the final run. In reality, the heights showed a continual increase. The vertical velocity used in the last run was such that rapid lifting of the inversion was forecast. Second, the surface winds which stayed strong even through the morning hours allowed more mixing in the lower layers thereby increasing the depth of the mixed layer. This is especially noticeable in the 13/1200 GMT surface wind (360 degrees at 2.1 m/s).

At Vandenberg AFB a small chain of mountains exists due-north of the base. With this northerly flow, there would be an increase in the local turbulence in the lower levels. Therefore, the poor height forecasts in this case is associated with the land influence which is not taken into account by the model.

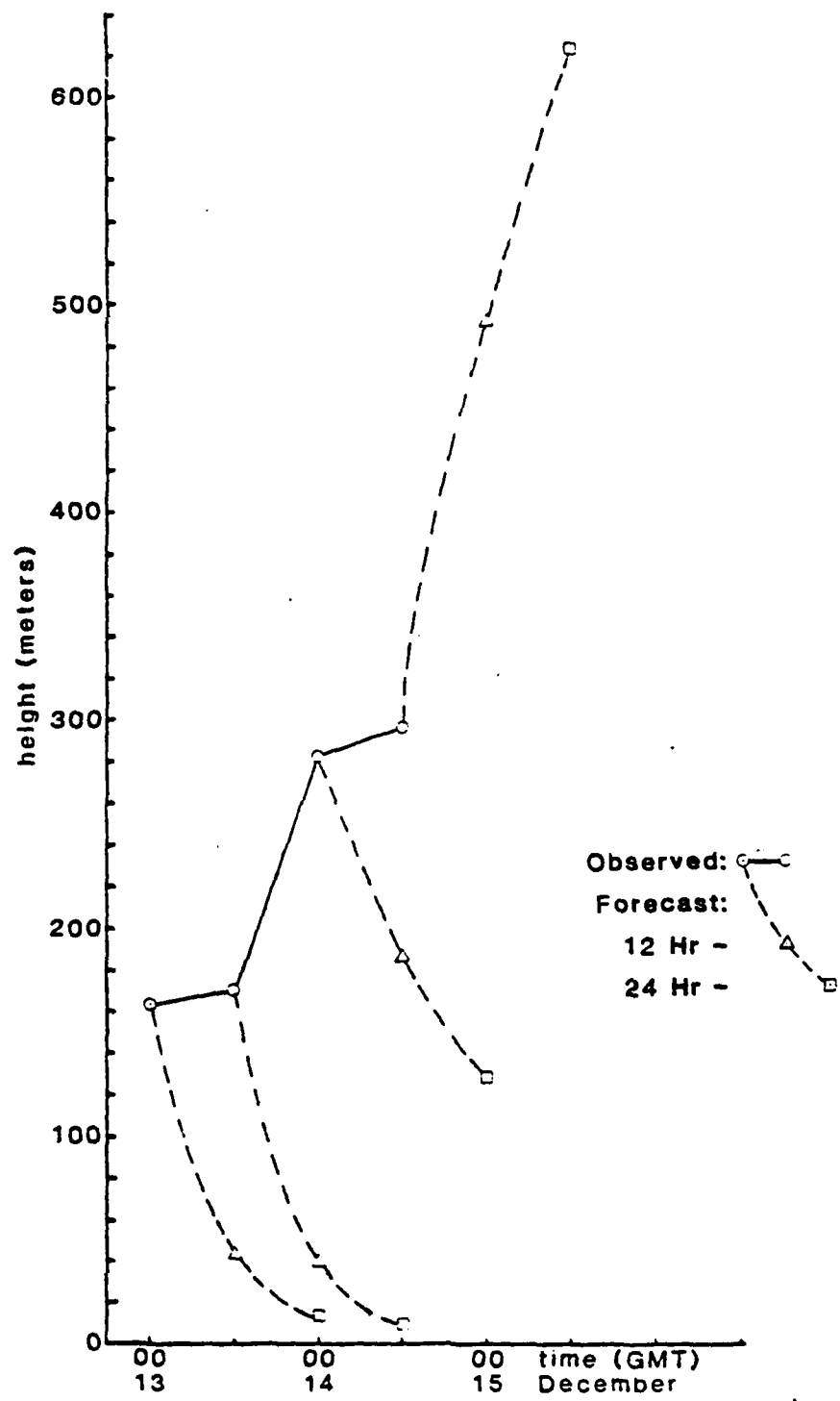


Figure 4.2 Graphical Depiction of Winter Case Observed and Forecasted Inversion Heights.

C. DISCUSSION OF MODEL RESULTS FOR PERIOD III (SPRING)

Tables X through XIII list the forecasted values for the spring case. This period was cloud free the first day and had low clouds the second. The forecasts did not include cloud formation until the third day. Even though the cloud forecasts were in error it does not appear that the cloud calculations had any real effect on the poor inversion height predictions.

The vertical velocities and entrainment rates were

TABLE X
April Inversion Results

DATE	GMT	OBS	FCST1	RMS	FCST2	RMS	FCST3	RMS
13	00	141	-	-	-	-	-	-
	12	136	31	105.0	-	-	-	-
14	00	289	9	295.0	75	214.0	-	-
	12	150	-	-	40	240.6	293	143.0
15	00	469	-	-	-	-	298	222.9
DATE	GMT	OBS	FCST4	RMS	FCST5	RMS	FCST6	RMS
15	00	469	140	329.0	-	-	-	-
	12	509	128	503.4	624	115.0	-	-
16	00	421	-	-	835	429.7	684	263.0
	12	291	-	-	-	-	867	663.2
DATE	GMT	OBS	FCST7	RMS	FCST8			
16	12	291	340	49.0	-			
	00	-	440	-	323			
	12	-	-	-	335			

different than those for other period. Entrainment rates were zero for the first and third forecasts, and the first three hours of the fifth forecast and were assigned a minimal positive value of .001. Hence, the inversion height was subsidence controlled for these times. The moisture forecasts were good since values agree to within 2 g/kg of the observed value and in some cases even less than 1 g/kg. Each of these forecasts were initialized with the evening sounding in which lifting condensation levels indicated no clouds.

TABLE XI
April Lifting Condensation Levels

DATE	GMT	OBS	FCST1	FCST2	FCST3	FCST4
13	00	705	-	-	-	-
	12	370	103	-	-	-
14	00	989	59	274	-	-
	12	305	-	191	919	-
15	00	506	-	-	861	234
	12	445	-	-	-	190
DATE	GMT	OBS	FCST5	FCST6	FCST7	FCST8
15	12	445	315	-	-	-
	00	623	423	398	-	-
16	12	256	-	303	297	-
	00	-	-	-	206	78
17	12	-	-	-	-	0

TABLE XII
April Potential Temperatures

DATE	GMT	OBS	FCST1	FCST2	FCST3	FCST4
13	00	13.6	-	-	-	-
	12	7.3	12.8	-	-	-
14	00	15.7	12.9	10.7	-	-
	12	8.2	-	12.5	15.1	-
15	00	13.2	-	-	14.7	10.3
	12	10.6	-	-	-	11.4
DATE	GMT	OBS	FCST5	FCST6	FCST7	FCST8
15	12	10.6	9.9	-	-	-
	00	12.4	9.6	8.7	-	-
16	12	8.3	-	7.1	12.3	-
	00	-	-	-	9.8	5.6
17	12	-	-	-	-	2.7

Close examination reveals that the potential temperature forecasts did not reflect the observed diurnal variation. The 12-hour forecast generally showed cooling or heating as it should but not sufficiently to agree with observed results. The 24-hour forecast tended to reverse the diurnal trend and to have cooling instead of heating or vice-versa.

It is believed that the land again influenced the observed inversion heights. Figure 4.3 shows the observed and forecasted inversion height values for this case. Close examination reveals that there appears to be two problems

TABLE XIII
April Moisture Values

DATE	GMT	OBS	FCST1	FCST2	FCST3	FCST4
13	00	6.6	-	-	-	-
	12	5.2	8.9	-	-	-
14	00	6.5	9.0	6.9	-	-
	12	5.7	-	8.2	6.5	-
15	00	7.2	-	-	6.6	6.8
	12	6.2	-	-	-	7.6
DATE	GMT	OBS	FCST5	FCST6	FCST7	FCST8
15	12	6.2	6.4	-	-	-
	00	6.4	5.9	5.6	-	-
16	12	5.9	-	5.3	7.6	-
	00	-	-	-	6.7	5.4
17	12	-	-	-	-	5.2

which are a combination of the problems discussed for the summer and winter cases. The first part of the period was strongly influenced by diurnal fluctuations and the forecasted values were similar to those in the summer case. The winter case was influenced by subsidence and surface winds. In this case, it is believed the northerly winds caused the increase in the observed inversion at 15/0000 GMT due to topographic induced large mechanical mixing. The vertical velocity allowed the model to decrease the heights for that time.

D. DISCUSSION OF MODEL RESULTS FOR PERIOD IV (FALL)

Tables XIV - XVII list the observed and forecasted values. As before predicted inversion heights for this case appear to be no better than those for previous cases. The formation of clouds was forecasted accurately since the model predicted cloud formation at a time when low clouds occurred in the area. However, forecasted lifting condensation levels were not in agreement with those observed.

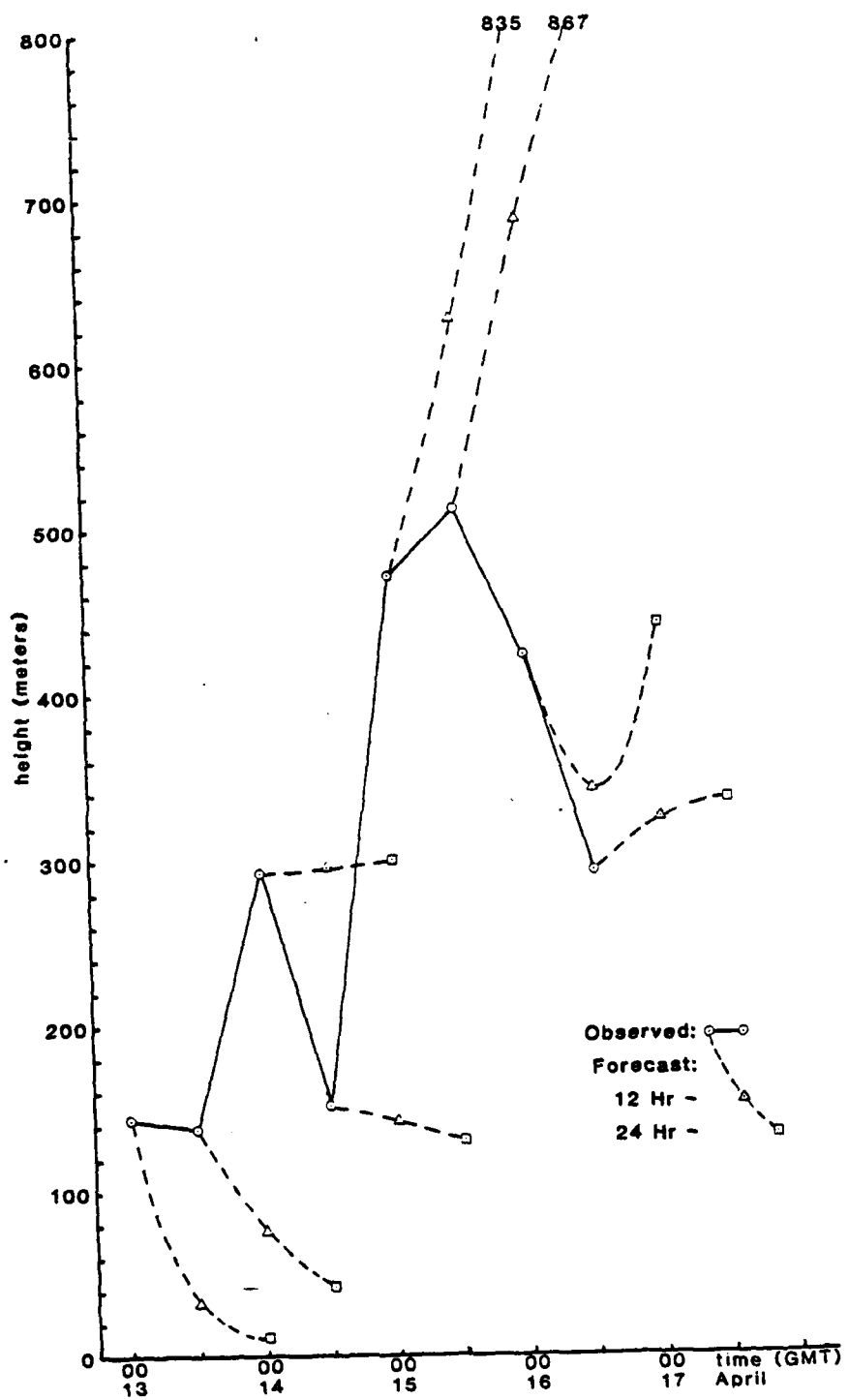


Figure 4.3 Graphical Depiction of Spring Case Observed and Forecasted Inversion Heights.

TABLE XIV
August-September Inversion Results

DATE	GMT	OBS	FCST1	RMS	FCST2	RMS	FCST3	RMS
29	00	287	-	-	-	-	-	-
	12	297	137	160.0	-	-	-	-
30	00	365	67	338.2	524	159.0	-	-
	12	311	-	-	638	363.6	383	72.0
31	00	391	-	-	-	-	496	127.3
DATE	GMT	OBS	FCST4	RMS	FCST5	RMS	FCST6	RMS
31	00	391	512	121.0	-	-	-	-
	12	553	666	165.6	574	21.0	-	-
1	00	322	-	-	755	433.5	819	497.0
	12	M	-	-	-	-	1057	-
DATE	GMT	OBS	FCST7	RMS	FCST8	RMS	FCST9	RMS
1	12	M	363	-	-	-	-	-
2	00	356	545	189.0	-	-	-	-
	12	356	-	-	273	83.0	-	-
3	00	411	-	-	225	244.2	449	38.0
	12	469	-	-	-	-	509	55.2
DATE	GMT	OBS	FCST10	RMS	FCST11	RMS	FCST12	RMS
3	12	469	491	22.0	-	-	-	-
4	00	422	714	292.8	684	262.0	-	-
	12	529	-	-	854	417.5	454	75.0
5	00	424	-	-	-	-	562	157.1
DATE	GMT	OBS	FCST13	RMS	FCST14	RMS	FCST15	
5	00	424	675	2510	-	-	-	
	12	429	823	467.2	404	25	-	
6	00	-	-	-	496	-	498	
	12	-	-	-	-	-	561	

The forecasted specific humidity values have an interesting trend (shown in Table XVII). Forecasts initialized from evening data were good but those initialized from morning data were bad. When initialized with evening data, the predicted specific humidity values were representative of the observed values. Obviously, poor forecasts of specific humidity or any other key parameter lead to poor prediction of inversion heights.

Potential temperatures, in all but two runs, were forecast to always decrease (cool) with time. The two morning to evening forecast cases did not reflect sufficient daytime heating, even with clouds present. To evaluate the poor

TABLE XIV
August-September Lifting Condensation Levels

DATE	GMT	OBS	FCST1	FCST2	FCST3	FCST4
29	00	781	-	-	-	-
	12	196	503	-	-	-
30	00	520	234	227	-	-
	12	206	-	0	78	-
31	00	406	-	-	0	297
	12	364	-	-	-	206
DATE	GMT	OBS	FCST5	FCST6	FCST7	FCST8
1	12	364	105	-	-	-
	00	467	227	613	-	-
2	12	M	-	580	101	-
	00	331	-	-	150	-
3	12	205	-	-	-	0
	00	577	-	-	-	0
DATE	GMT	OBS	FCST9	FCST10	FCST11	FCST12
3	00	577	237	-	-	-
	12	284	122	325	-	-
4	00	496	-	452	424	-
	12	452	-	-	341	0
5	00	525	-	-	-	-
	12	-	-	-	-	0
DATE	GMT	OBS	FCST13	FCST14	FCST15	
5	00	525	374	-	-	
	12	310	263	394	-	
6	00	-	-	186	194	
	12	-	-	-	0	

performance in potential temperature forecasts, the subsidence rates, specific humidity and diurnal radiation variations were compared. When the forecast was for a morning to evening period, excluding the two previously mentioned forecasts, continued cooling was predicted when heating should have been predicted. This result was independent of subsidence rates or presence of clouds. Therefore, for morning to evening forecasts, radiation effects were not sufficient to introduce the needed daytime heating. From evening to morning the major problem was too much cooling. This happened in five of the forecasts with another five forecasts showing good cooling rates but bad forecasts for the 24-hour point since the previous 12-hour forecast was bad. The good cooling rates occurred when the subsidence was at its largest compared to the excessive lowering forecasts. This would indicate possible problems in the radiation

TABLE XVI
August-September Potential Temperatures

DATE	GMT	OBS	FCST1	FCST2	FCST3	FCST4
29	00	17.8	-	-	-	-
	12	13.5	16.6	-	-	-
30	00	16.8	15.5	10.4	-	-
	12	13.8	-	7.6	13.7	-
31	00	15.6	-	-	11.5	9.8
	12	14.2	-	-	-	7.6
DATE	GMT	OBS	FCST5	FCST6	FCST7	FCST8
31	12	14.2	12.3	-	-	-
	00	17.6	13.2	12.1	-	-
1	12	M	-	10.3	13.8	-
	00	16.1	-	-	12.5	-
2	12	12.8	-	-	-	8.6
	00	15.4	-	-	-	9.7
DATE	GMT	OBS	FCST9	FCST10	FCST11	FCST12
3	00	15.4	9.9	-	-	-
	12	13.1	7.8	12.2	-	-
4	00	16.0	-	10.8	10.1	-
	12	14.1	-	-	7.9	12.2
5	00	16.6	-	-	-	11.2
	12	-	-	-	-	-
DATE	GMT	OBS	FCST13	FCST14	FCST15	
5	00	16.6	11.6	-	-	
	12	13.8	9.7	16.1	-	
6	00	-	-	12.8	11.2	
	12	-	-	-	8.7	

segment which would be cooling the potential temperatures for this time of day.

Figure 4.4 shows the observed and forecasted inversions for this period. Key factors affecting inversion heights during this period were diurnal heating variations, surface winds, and clouds. The temperatures showed a definite diurnal pattern throughout the period as did the lifting condensation level. The inversion displayed a diurnal trend only part of the time, 29/1200 GMT through 31/0000 GMT and 3/0000 GMT through the remainder of the period.

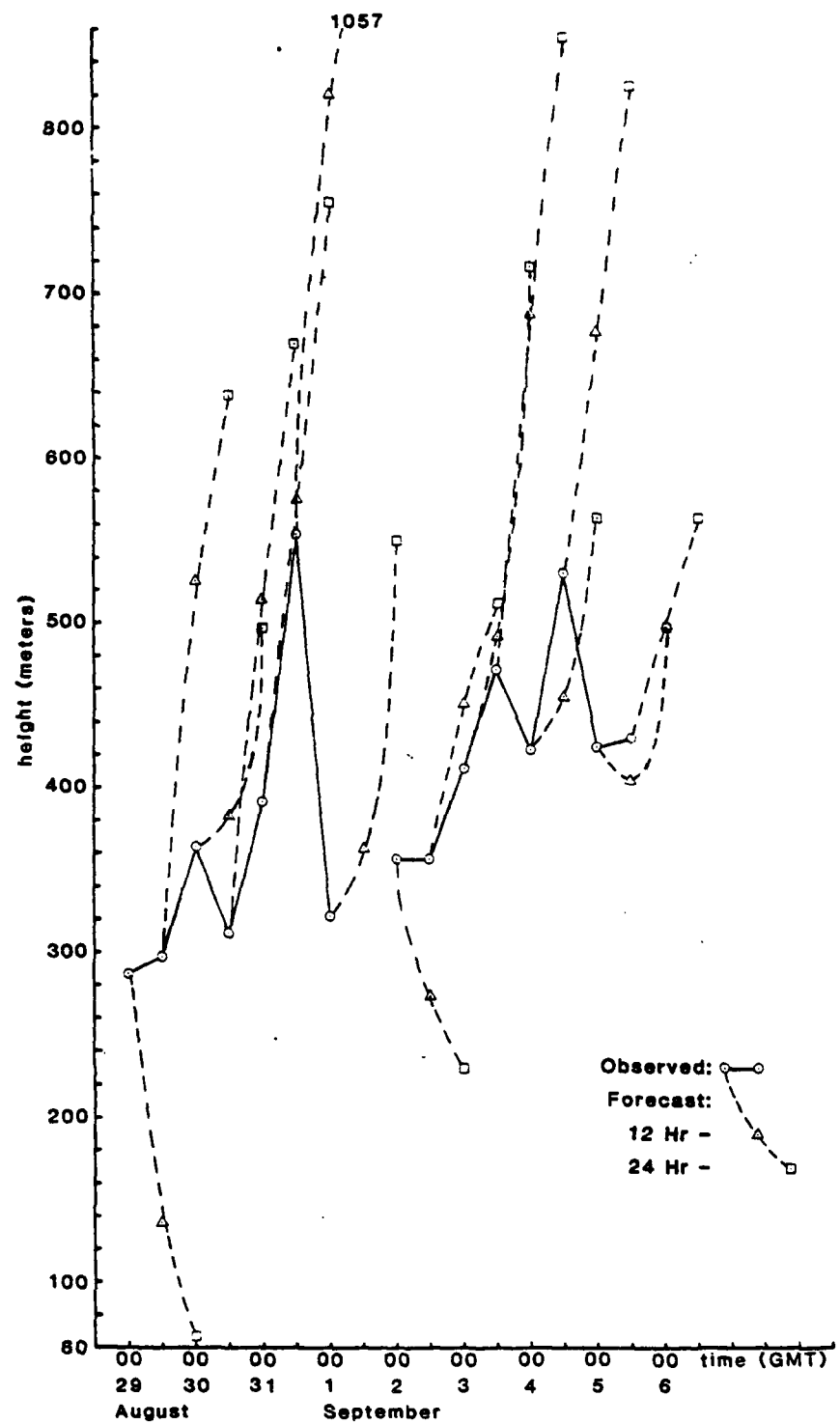
The low subsidence values contributed greatly to the high inversion height values forecasted during this period. Of the remaining forecasts, those with heights forecast to decrease were evening to morning forecasts with subsidence occurring. The observed heights increased (except for the 2/0000 GMT value which remained constant) due to strong

TABLE XVII
August-September Moisture Values

DATE	GMT	OBS	FCST1	FCST2	FCST3	FCST4
29	00	8.5	-	-	-	-
	12	8.7	9.0	-	-	-
30	00	9.1	9.7	6.9	-	-
	12	8.8	-	6.6	9.3	-
31	00	9.0	-	-	9.3	6.4
	12	8.3	-	-	-	5.8
DATE	GMT	OBS	FCST5	FCST6	FCST7	FCST8
1	12	8.3	8.4	-	-	-
	00	9.9	8.3	6.3	-	-
2	12	M	-	5.7	9.3	-
	00	9.6	-	-	8.3	-
3	12	8.2	-	-	-	9.1
	00	8.0	-	-	-	8.9
DATE	GMT	OBS	FCST9	FCST10	FCST11	FCST12
3	00	8.0	6.7	-	-	-
	12	8.1	6.1	7.4	-	-
4	00	8.7	-	6.3	6.1	-
	12	7.9	-	-	5.5	9.0
5	00	9.0	-	-	-	9.1
DATE	GMT	OBS	FCST13	FCST14	FCST15	
5	00	9.0	6.9	-	-	
	12	8.3	6.4	9.3	-	
6	00	-	-	8.3	7.5	
	12	-	-	-	7.0	

winds (weaker and more westerly at 2/0000 GMT) which lifted the inversion due to mixing.

At 31/1200 GMT an observed height decrease occurred for the morning to evening forecast time but the forecasts showed rises. To explain this requires consideration of all three factors mentioned above. The observed height values decreased due to the increase in cloud coverage and continued onshore flow whereas the normal situation is offshore flow due to diurnal changes. The radiation computations also appear to have been responsible for errors in the forecasts for this period. Radiation was not the only problem since erroneous specific humidity and vertical velocities contributed. There was land influence on the parameters involved in height predictions, as in the other cases.



E. SUMMARY AND GENERAL COMMENTS

It is easily seen by the large root mean square scores and the large differences between forecast and observed trends, depicted graphically, that the model did not yield a good prediction of inversion heights at Vandenberg AFB. The model also did not yield very good forecasts of the other parameters.

The discussions present an explanation of the probable components where errors occurred. There are certain prime factors which cause the greatest problem. The largest error producer is the fact that Vandenberg AFB is a land base which strongly experiences diurnal variations in temperature and winds. The primary predictive values of the model (subsidence, entrainment, radiation and presence of clouds) are also influenced by the land effect. Daytime heating which increases temperature and, hence, dissipates clouds is not accounted for in the MAEL model.

Topography and certain wind directions increase the turbulence in the mixed layer. With mountains north as well as south of Vandenberg AFB, this condition can result when the offshore flow does not set up during the night and strong northerly or southerly flow continues. This leads to deepening of the mixed layer and can overcome the effects of subsidence. The result of this would be to lift instead of lower the inversion.

It is concluded that this study yielded conclusive evidence that the MAEL model is not appropriate for use at a coastal station because, even though coastal, land influences play a significant role. The results from the study by Gleason (1982) reveals definite contrasts with this one. He had good results for San Nicolas Island and was able to show that the Q-method of calculating vertical velocities was best.

V. SUMMARY AND CONCLUSIONS

Accurate predictions of variations in the height of atmospheric inversions are a necessity in proper usage of modern weaponry. This is because of the impact changes in inversion heights have on the ducting of weapons guidance system or of tracking system signals. Atmospheric parameters are continually changing and those parameters which govern inversions can easily change their entire profile in a matter of hours. Forecasts of changes in inversion properties must start with forecasts of those parameters, namely, temperature and specific humidity. To do this the marine atmospheric boundary layer model used at the Naval Postgraduate School was utilized.

Data periods which covered each season were chosen for the Vandenberg AFB area. All four cases were dominated by a high pressure system over the eastern North Pacific Ocean. Clear as well as cloudy days were considered to allow full range testing for a station strongly influenced by land conditions. Data for these periods were from rawinsonde observations, satellite information, and surface and 500 mb synoptic analyses. Model input parameters were from the rawinsonde observations and satellite derived sea-surface temperatures.

Results from each model run were compared with observed values to determine accuracies of the model. It was found that the model did not yield accurate predictions during most of the cases. Final interpretations of these inaccuracies always point to strong land influence. Diurnal variations influenced by the land are much greater than variations over water and are not reflected in the model calculations.

The end result of this study is that this MABL model does not work for Vandenberg AFB. It is not currently valid for statics strongly influenced by land induced diurnal variations. The redevelopment of the model to treat such factors is required to properly handle the land influences.

LIST OF REFERENCES

Davidson, K. L., C. W. Fairall, P. Jones Boyle, and G. E. Schacher, 1984: Verification of an atmospheric mixed layer model for a coastal region. In publication: J. of Climate and Appl. Meteor.

_____, and R. W. Garwood, 1984: Coupled oceanic and atmospheric mixed layer model. In publication: Dynamics of Atmos. and Ocean.

Fleagle, R., and J. A. Businger, 1980: An Introduction to Atmospheric Physics, 2d ed., Academic Press, 432 pp.

Gleason, J. P., 1982: Single-station assessments of the synoptic-scale forcing on the marine atmospheric boundary layer. NPS Master's Thesis (K. L. Davidson, advisor), Naval Postgraduate School, Monterey, CA., 57 pp.

Haggerty, J. A., 1983: Entrainment of Pollutants into a Cloud-topped Marine Boundary Layer. Master's Thesis, University of California, Davis, 102 pp.

Stage, S. A., and J. A. Businger, 1981: A model for entrainment into a cloud topped marine boundary layer. Part I: Model description and application to a cold-air outbreak episode. J. Atmos. Sci., 38: 2213-2229.

INITIAL DISTRIBUTION LIST

	No. Copies
1. Defense Technical Information Center Cameron Station Alexandria, Virginia 22314	2
2. Library, Code 0142 Naval Postgraduate School Monterey, California 93943	2
3. Commander Naval Oceanography Command NSTL Station, Mississippi 39529	1
4. Commanding Officer Fleet Numerical Oceanography Center Monterey, California 93943	1
5. Officer-in-Charge Naval Environmental Prediction Research Facility Monterey, California 93943	1
6. Prof. R. J. Renard, Code 63RD Naval Postgraduate School Monterey, California 93943	1
7. Prof. C. N. K. Mooers, Code 68MR Naval Postgraduate School Monterey, California 93943	1
8. Department of Meteorology Library, Code 63 Naval Postgraduate School Monterey, California 93943	1
9. Major Patrick Herod AFIT/CIRF Wright-Patterson AFB, Ohio 45433	2
10. Air Weather Service Technical Library Scott AFB, Illinois 62225	1
11. Atmospheric Sciences Lab DEIAS-AS-P White Sands Missile Range, New Mexico 88002	1
12. Captain Richard B. Wilkerson FSC 2032 Scott AFB, IL 62225	1
13. Director of Research and Administration Code 012 Naval Postgraduate School Monterey, California 93943	1
14. Dr. C. W. Fairall Department of Meteorology Walker Building Pennsylvania State University University Park, Pennsylvania 16802	1

15.	Prof. K. L. Davidson, Code 63Ds Naval Postgraduate School Monterey California 93943	10
16.	Prof. G. E. Schacher, Code 61Sq Naval Postgraduate School Monterey California 93943	1
18.	Capt K. Van Sickle Commander Naval Environmental Prediction Research Facility Monterey California 93943	1
19.	DR. Barry Katz Code R42 Naval Surface Weapons Center White Oak Laboratory Silver Spring, Maryland 20362	1
20.	Dr. J. H. Richter Code 532 Naval Ocean Systems Center San Diego, California 92152	1
21.	Dr. Lothar Ruhnke Code 8320 Naval Research Laboratory Washington D.C. 20375	1
22.	Commander Fet 30, 2 Wea. Sq. Vandenberg AFB, Ca. 93437	1

END